ABSTRACT

Title of thesis: REACTION NETWORK ANALYSIS FOR THIN FILM DEPOSITION PROCESSES

Krishnaprasath Ramakrishnasubramanian
Master of Science, 2016

Thesis directed by: Professor Raymond A. Adomaitis
Department of Chemical and Biomolecular Engineering

Understanding the growth of thin films produced by Atomic Layer Deposition (ALD) and Chemical Vapor Deposition (CVD) has been one of the most important challenge for surface chemists over the last two to three decades. There has been a lack of complete understanding of the surface chemistry behind these systems due to the dearth of experimental reaction kinetics data available. The data that do exist are generally derived through quantum computations. Thus, it becomes ever so important to develop a deposition model which not only predicts the bulk film chemistry but also explains its self-limiting nature and growth surface stability without the use of reaction rate data.

The reaction network analysis tools developed in this thesis are based on a reaction factorization approach that aims to decouple the reaction rates by accounting for the chemical species surface balance dynamic equations. This process eliminates the redundant dynamic modes and identifies conserved modes as reaction invariants. The analysis of these invariants is carried out using a Species-Reaction (S-R) graph

approach which also serves to simplify the representation of the complex reaction network. The S-R graph is self explanatory and consistent for all systems. The invariants can be easily extracted from the S-R graph by following a set of straightforward rules and this is demonstrated for the CVD of gallium nitride and the ALD of gallium arsenide. We propose that understanding invariants through these S-R graphs not only provides us with the physical significance of conserved modes but also give us a better insight into the deposition mechanism.

REACTION NETWORK ANALYSIS FOR THIN FILM DEPOSITION PROCESSES

by

Krishnaprasath Ramakrishnasubramanian

Thesis submitted to the Faculty of the Graduate School of the
University of Maryland, College Park in partial fulfillment
of the requirements for the degree of
Master of Science
2016

Advisory Committee:
Dr Raymond Adomaitis/Advisor
Dr Dongxia Liu
Dr Sheryl Ehrman

Acknowledgments

I owe my gratitude to all the people who have made this thesis possible and who made my graduate experience one that I will cherish forever.

First and foremost I would like to thank my advisor, Professor Raymond Adomaitis for giving me the opportunity to work on some extremely interesting projects over the past two and half years. He has always welcomed me with a smile when my research work gets stuck and has made sure I leave the room with smile, answers and lots of ideas.

I would also like to thank my research group mate, my troubleshooter!, a close friend and a great individual Hossein Salami for all his help and ideas. Our thoughtful discussions are something that has gone a long way in shaping my research thinking skills.

I owe my deepest thanks to my family. My mother, for reminding me to smile and not take it all too seriously. My father, who has always supported my decisions and my brother for always encouraging me on my journey. Words cannot express the gratitude I owe them.

I have never realized that I live so far away from home thanks to my friends Akshay, Sujay, Nithya, Abhijith, Madhu, Nikhil, Naresh, Sai, Soumya who made sure I remain myself admist all the vicissitudes of life. Whether to sit with me and eat bowls of ice cream in the middle of the night or, to feed me massive amounts of food or just to sit and laugh all day long, Thanks for being there for me. Lastly, thank god for giving me such a wonderful life!.

Table of Contents

List of Tables

List of Figures

Chapter 1: Introduction

1.1 Motivation

The motivation to study III-V compound semiconductor materials stems from their importance in optoelectronics. It is this application that distinguishes them greatly from Si based devices. Along with having the advantage of being a direct band gap (unlike silicon), gallium nitride (GaN), one of the most widely used III-V semiconductor also has a wide band gap and high breakdown field properties thus making it the ideal material for Light Emitting Diodes (LED) manufacturing [Bandic et al., 1998]. In addition, GaN based devices are also used in high frequency and high power applications [Burk et al., 1999].

The other most important III-V compound semiconductor is gallium arsenide (GaAs). In the early 90's GaAs was hailed as the future of microelectronics before it faded away due to its high manufacturing cost compared to silicon. However, its application in the solar industry for making High Concentration Photovoltaics (HCPV) is gaining prominence. Also, the high electron mobility property of GaAs is one of the main reasons why it is used in transistors that achieve high gain at high bandwidth. It is thus no wonder GaAs is an indispensable part of our RF based high-end Wifi receivers and transmitters, and is almost certainly at the heart of our

cell phone's receivers and transmitters. A report published by Information Network predicts the "GaAs IC market to grow to 8 Billion USD in 2017", which further asserts our goal to better understand GaAs deposition.

Metal Organic Chemical Vapor Epitaxy (MOVPE) or MOCVD is the technique used to grow crystalline layers of gallium nitride [Theodoropoulos et al., 2001]. There are a large number of gas phase and surface reactions that take place in a GaN MOCVD reactor. When some believe that complex gas phase reactions are largely responsible for generating the main deposition species [Pawlowski et al., 2000] other research groups consider only surface reactions in modeling their deposition chemistry [Safvi et al., 1997][Mihopoulos, 1999]. The difficulty in reaching a consistent mechanism can largely be attributed to the complex chemistry of the deposition process.

The same is true for the Atomic Layer Deposition (ALD) of GaAs. Even though there have been numerous research studies on GaAs deposition kinetics over the last two decades, they have failed to develop a consistent model for its self-limiting growth. Tischler and Bedair [Tischler and Bedair, 1986] worked on understanding the self limiting growth by varying the moles of the precursor and observing that the growth became independent of the amount of precursor. Yu [Yu, 1993] identified similar behavior by developing a numerical model for the deposition. Creighton and Bansenauer [Creighton and Bansenauer, 1993] of the Sandia National Laboratories proposed possible explanations for the ideal monolayer growth but did not give a detailed surface mechanism. Thus, we propose deposition mechanisms for the CVD of GaN and the ALD of GaAs before analyzing their

accuracy through our Reaction Network Analysis (RNA) tools. We have developed Gauss-jordan factorization based approach to decouple the nonlinear reaction rates to identify the conserved quantities followed by detailed analysis of our conserved quantities through the use of Species-Reaction (S-R) graph providing us with a physical meaning for these invariants and also a better insight into the accuracy of our proposed reaction mechanisms.

1.2 Chemical Vapor Deposition and Atomic Layer Deposition

In Chemical Vapor Deposition (CVD) process one or more gaseous precursors are injected into a reactor which contains a heated substrate on which thin-film depostion takes place. In epitaxial MOCVD process, temperature of the substrate is usually above 1000 °C and so results in a large network of gas phase thermal decomposition reactions. Metal Organic Chemical Vapor Deposition (MOCVD) refers to those processes where one of the precursor is an organometallic compound (TMGa, TMA etc). MOCVD is widely used in industry to grow layers of crystalline thin film. Due to the array of gas phase decompositions reactions, the film quality can be difficult to control.

Atomic Layer Deposition (ALD) is a type of CVD technique which is used to grow films with precise thickness by controlling growth at the atomic level. Almost all of ALD techniques have two precursor gases which are alternatively fed into the reactor. A purge stream is used to evacuate gases that are not absorbed. One of the advantages of ALD over CVD is its self-limiting nature which makes the process less

sensitive to process conditions variations. This results in conformality of high aspect ratio structures and also growth of structured 3D materials [Johnson et al., 2014]. The self-limiting nature is caused by the limited number of reactive surface sites and the presence of bulky ligand groups on the surface. Thus, even though the layer by layer deposition takes longer compared to the CVD, ALD is used for producing highly quality films at a low temperature. Such features are essential for coating heat-sensitive materials [Pinna and Knez, 2011]. In this thesis we study one example each for the CVD and the ALD processes.

1.3 Reaction Network Analysis

The idea of Reaction Network Analysis (RNA) is useful for understanding thin-film deposition systems. If the challenge in a steady state CVD process is to identify the primary set of gas phase reactions that influence the surface reactions, an ALD system requires development of the correct kinetic models of the surface reactions to match the growth per cycle (gpc) from experiments. However, the important hurdle in both the cases is the lack of reaction rate data to model deposition dynamics. Thus, before performing Density Functional Theory (DFT) studies or *Ab inito* calculations to calculate the rates, it becomes important to understand whether the mechnanism proposed is a "proper" ALD or CVD mechanism. The definition of "proper" is made much clearer in the Objective section. This thesis evaluates the deposition mechanisms we have developed through the reaction factorization approach. It was developed by [Adomaitis, 2016b] [Adomaitis, 2016a] to

decouple the non linear reaction modes and determine the reaction invariants. This analysis of the reaction network is further extended though the use of S-R graph, which is the representation of the main elements of a reaction network in terms of a graph. The S-R graph was orginally developed by [Craciun and Feinberg, 2006] who applied it to represent multiple equllibrium in chemical reaction networks. We have extended this idea to answer important questions in thin-film deposition processes by developing a set of guidelines and rules to help in extracting reaction invariants. By directly generating these invariants from the S-R graph we can quickly identify if the mechanism is complete before investing significant time and effort in determining its reaction rates.

1.4 Objective of this thesis

Due to large dearth in the availability of surface kinetic data associated with most of the ALD and CVD processes it becomes important to develop a reaction mechanism which can be supported by a factor other than experimental kinetics data. It is at this point that we believe our RNA tools will be helpful in identifying whether our mechanism is a "proper" ALD or CVD. The objectives of the thesis is to develop a complete set of RNA tools that can answer the following questions which satisfy our idea of a "proper" ALD or CVD:

- Can the reaction time scales (finite and equilibrium) involved in our mecahnism can be separated?
- Can RNA verify if the ALD mechanism proposed is self-limiting in nature?

- Will the the stoichiometry of the deposited film be independent of the reaction-rate values?

- Is the overall RN balanced in terms of satisfying all the individual elemental balances during the original state as well as during the transition states?

- Will our network give us an insight into the surface stability of the deposition process and will each of the mode identified as redundant have a physical meaning associated with it?

The factorization approach is used to decouple the reaction rates and identify process invariants while the S-R graph approach is used to understand the physical significance of these invariants. We apply the RNA tools on a GaAs film deposited by ALD and a GaN deposited through CVD in order to identify the physcial meaning of the respective invariants before drawing a comaprison between their characteristic properties.

Chapter 2: Reaction Network for III-V Compound Semiconductor Systems

2.1 Overview of GaAs

GaAs is one of the most important III-V semiconductor material grown from trimethyl gallium (TMGa) and arsine (AsH_3) precursors. It has a band gap value of 1.424 eV (at 300 K) and is used for the manufacture of infrared LED's. It has a zinc blende structure, hence each atom is four coordinated and has a local tetrahedral geometry. ALD of GaAs is generally carried out in flow systems operating between atmospheric and 20 Torr pressure [Kaariainen et al., 2013]. However, there has also been growth of ALD in UHV systems with the precursors exposed to the substrate alternatively before being removed by a vacuum pump. Sometimes a purge gas is also used to evacuate the chamber. The thickness of 1 monolayer (ML) is 2.83 Åwhich is the expected growth per cycle (gpc) at saturation. Reactor temperature is typically 500 K and at higher temperatures we find thermal decomposition of the gas precursors results in > 1 ML growth.

2.2 Reaction mechanism for the ALD of GaAs

Most ALD process requires two gaseous precursors, in the case of GaAs we have trimethyl gallium (TMGa) and arsine (AsH_3). Surface mechanisms for the ALD of GaAs have been studied by many researchers. It is well accepted that the process begins with the chemi-adsorption of the TMGa precursor on an arsenic terminated GaAs surface. Yu et al [Yu, 1993] has performed mass spectrometry studies to show the saturation of the gallium surface by methyl groups for achieving self limiting growth. Creighton and Bansenauer [Creighton and Bansenauer, 1993] proposed an adsorbate inhibition mechanism to show presence of methyl groups on the surface in support of monolayer growth. Experimental evidence from performing surface chemistry study has shown that CH_3 is the primary species for terminating a galliuim rich surface to achieve self-limiting monolayer growth [Kaariainen et al., 2013], [Ars et al., 1998].

Nishizawa et al [Nishiwaza et al., 1987] have demonstrated that at a TMGa pressure of 5×10^{-4} Torr and 4 s exposure per cycle, close to a monolayer (ML) of GaAs, could be deposited per growth cycle when the reaction temperature was in the vicinity of 500 °C. The self-limiting deposition of Ga was evidenced by the fact that the growth per cycle was independent of the TMGa dosage once the latter exceeded a minimum value to produce a monolayer. Temperature was a very important parameter since higher temperatures yielded > 1 monolayer growth. Mass spectroscopy studies from Nishizawa's group has also shown the presence of CH_4 in the gas phase which supports the H-transfer mechanism. However, alternate

results of CH_3 desorption without H-transfer has also been reported by Maa et al [Maa and Dapkus, 1993] through performing reflectance difference spectroscopy (RDS) and sampled beam mass spectroscopy studies. The reaction mechanism proposed in our study is however based on this H-transfer mechanism. We assume that the initial GaAs surface is arsenic rich and each of these surface arsenic atoms are terminated by two hydrogens. We perform density of sites calculations in the Appendix A to support our assumption of a single methyl terminated gallium site then a gallium terminated by two methyl groups. Our proposed mechanism can be broken down into two half cycles.

2.2.1 First Half Cycle

In the first half cycle, the TMGa precursor is adsorbed on the arsenic rich surface. The arsenic atom has a lone pair of electrons which acts as the adsorption site for the precursor with an empty p-orbital. After the arsenic is adsorbed on the surface it forms a complex as shown in Figure 2.1.

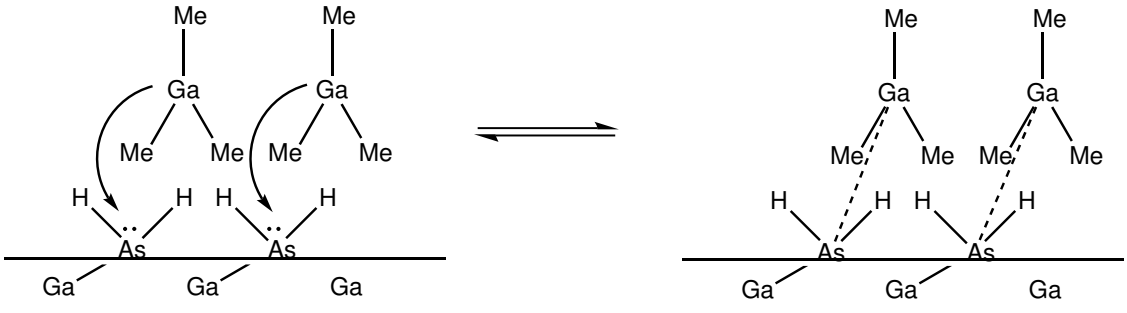

Figure 2.1: Adsorption of the TMG on the arsenic surface site

Then the hydrogen on the surface arsenic undergoes a (1-2) H-transfer and

is removed along with the methyl group as methane through the formation of a transistion state as shown in Figure 2.2 and Figure 2.3.

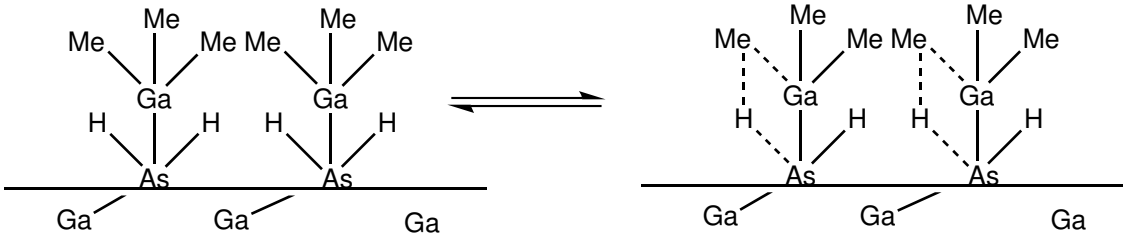

Figure 2.2: Formation of transistion state for elimination of methane

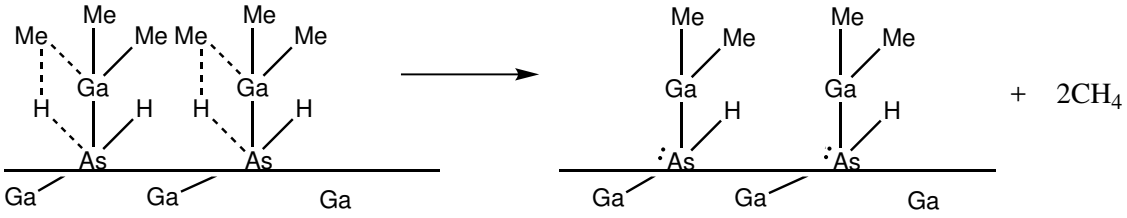

Figure 2.3: Stable indermediate after elimination of methane.

In the exact sequence as the previous steps, another methyl group on the gallium atom is removed through a proton transfer with the arsenic hydrogen.

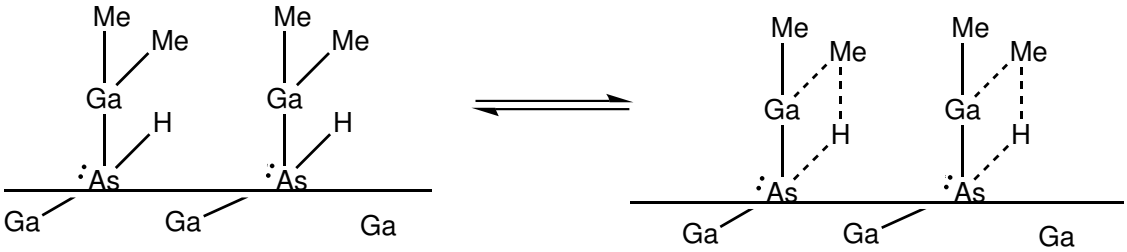

Figure 2.4: Transistion state for the elimination of another methane.

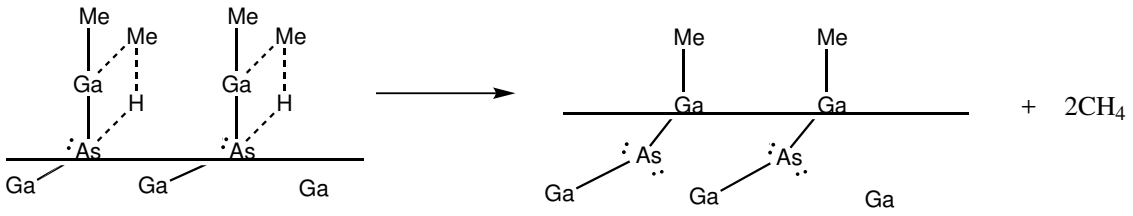

Figure 2.5: Stable indermediate at the end of first cycle

2.2.2 Second Half Cycle

Now the Ga has an empty orbital which can act as a reactive site for the second half cycle. The second half cycle begins with the arsine pulse. This AsH_3 has a lone pair of electrons and hence is chemisorbed on the Ga-rich surface as shown in Figure A.4. It is also important to note that the gallium on the surface now has just one methyl group attached to it as shown in Figure 2.5. The hydrogen on the arsenic atom undergoes a proton transfer and is removed as CH_4 along with the methyl group on the surface. These are elementary reactions that occur through the formation of a transition state as shown in Figure 2.7 and Figure 2.8. The entire reaction mechanism is summarized in Table 2.1

Figure 2.6: Arsenic adsoption on the gallium surface terminated by methyl groups.

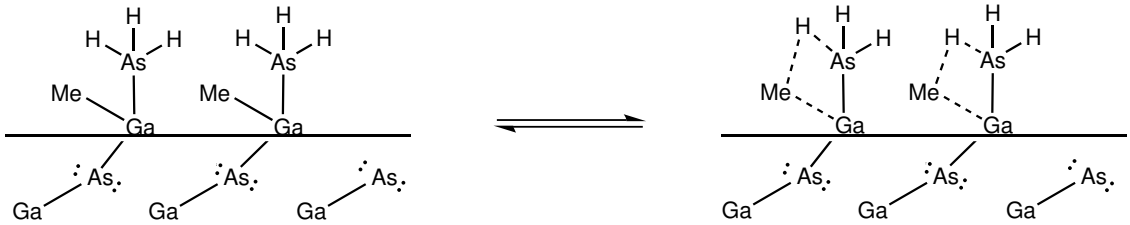

Figure 2.7: Transistion state for elimination of methane

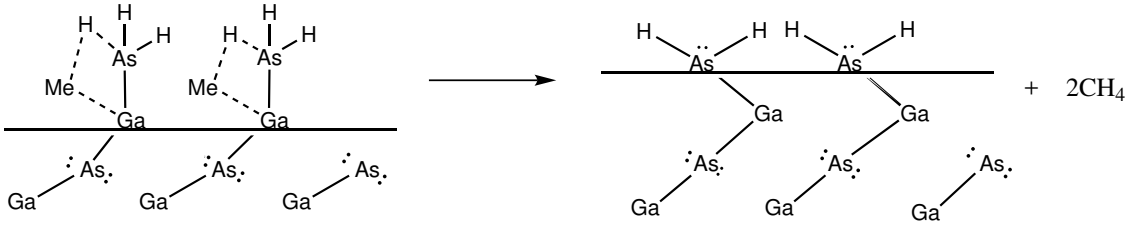

Figure 2.8: Deposition of bulk GaAs with regeneration arsenic site

2.2.3 Reaction Network for GaAs ALD

Table 2.1: Reaction summary for GaAs ALD

Reaction	Rate ($s^{-1}m^{-2}$)
$AsH_2 + GaMe_3$ (g) + 3S $\longrightarrow$ AsH_2GaMe_3	f_0
$AsH_2GaMe_3 \rightleftharpoons AsH_2GaMe_3^*$	$(1/\epsilon)g_0$
$AsH_2GaMe_3^* \longrightarrow AsHGaMe_2 + CH_4$ (g) + S	f_1
$AsHGaMe_2 \rightleftharpoons AsHGaMe_2^*$	$(1/\epsilon)g_1$
$AsHGaMe_2^* \longrightarrow$ As (b) + GaMe + CH_4 (g) + S	f_2
GaMe + AsH_3 (g) $\longrightarrow$ $GaMeAsH_3$	f_3
$GaMeAsH_3 \rightleftharpoons GaMeAsH_3^*$	$(1/\epsilon)g_2$
$GaMeAsH_3^* \longrightarrow$ Ga (b) + AsH_2 + CH_4 (g) + S	f_4

The one factor that shows up on the reaction mechanism is the factor 'S' which is a pseudo-species. It is called the surface site, whenever a methyl group is consumed the factor 'S' is added to the reactant side and whenever a methyl is released as methane we add the factor to the product side. 'S' refers to space that is consumed by a methyl group. Due to the presence of a bulky methyl group a possible reactive site is left unreacted or "inaccessible". Thus, an ALD process with sub monolayer growth can be explained using the presence of excessive methyl groups (or any ligands!).

2.3 Overview of GaN

GaN is generally grown from trimethyl gallium (TMGa) and ammonia as precursors. Unlike ALD both the precursors are injected into the reactor at the same time. GaN has a band gap value of 3.4 eV making it most suitable for optoelectronic's and mainly for the manufacture of commercial LED's. It is typically grown over a sapphire substrate by MOCVD. The temperature of typical GaN deposition is around 1000 °C and hydrogen can be used as a carrier gas with 25-760 Torr pressure. GaN forms a wurtzite structure which has a coordination number of four for both Ga and N.

2.4 Reaction mechanism for the CVD of GaN

The reaction mechanism for a CVD is far different from that of an ALD process. Firstly because both precursors are fed into the system simultaneously,

gas phase reactions can form adducts [Almond et al., 1992, Mazzarese et al., 1989]. These adducts decompose to give methane and dimethylgallium amide ($(CH_3)_2GaNH_2$). What happens after this step is not clearly understood. Many mechanisms have proposed a formation of a six member trimer complex through oligomerization [Theodoropoulos et al., 2001, Pawlowski et al., 2000, Safvi et al., 1997] [Mihopoulos, 1999, Sun et al., 1999, Sun et al., 2000, Parikh and Adomaitis, 2006]. In our mechanism, we however assume that due to complexities for a ring adsorption on the surface, only the monomer species adsorbs. The idea of GaN film growth with the adsorption of a monomer is valid only at temperatures less than 900 °C, thus our mechanism explains low temperature CVD systems. However, due to the relatively higher temperature of the substrate we need to define our surface sites carefully. Unlike the ALD case here we assume a surface which is bare gallium with nothing attached to it. The entire reaction mechanism is then summarized in Table 2.2

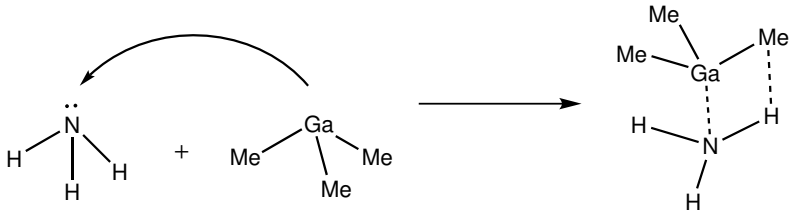

Figure 2.9: Reaction between gas phase precursors

2.4.1 Reaction Network for GaN CVD

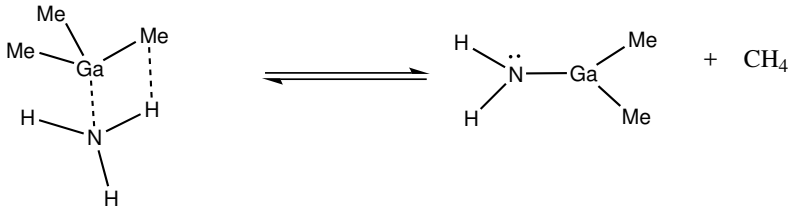

Figure 2.10: Methane elimination resulting in dimethylgallium amide

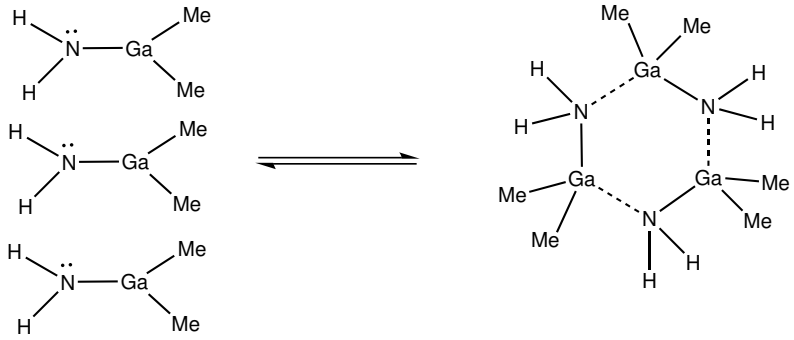

Figure 2.11: Formation of six member trimer species

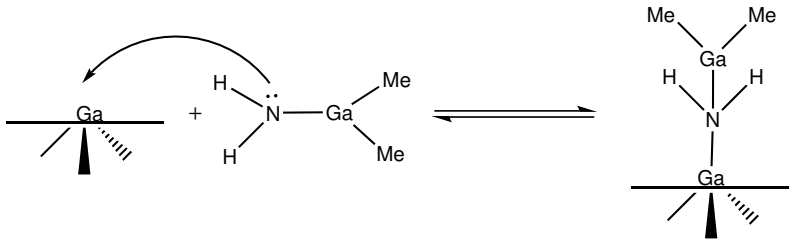

Figure 2.12: Adsorption of the monomer in the gas phase onto the gallium surface

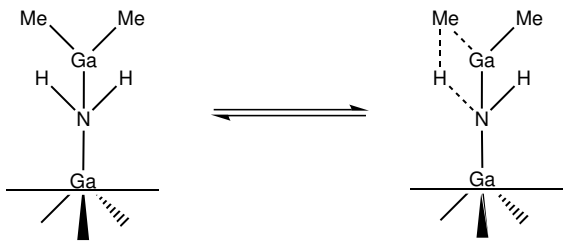

Figure 2.13: Transistion state formation prior to methane elimination

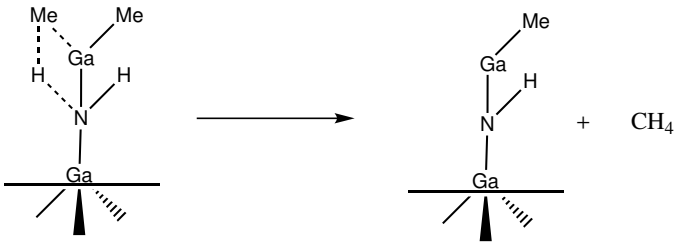

Figure 2.14: Elimination of methane to yield an intermediate on the surface

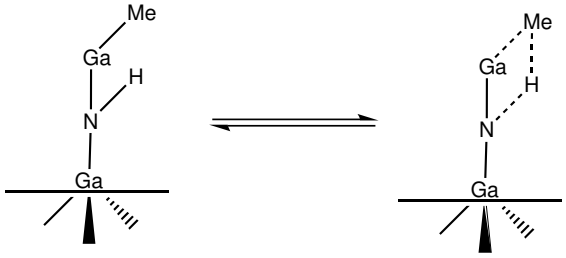

Figure 2.15: Transistion state formation prior to second methane elimination

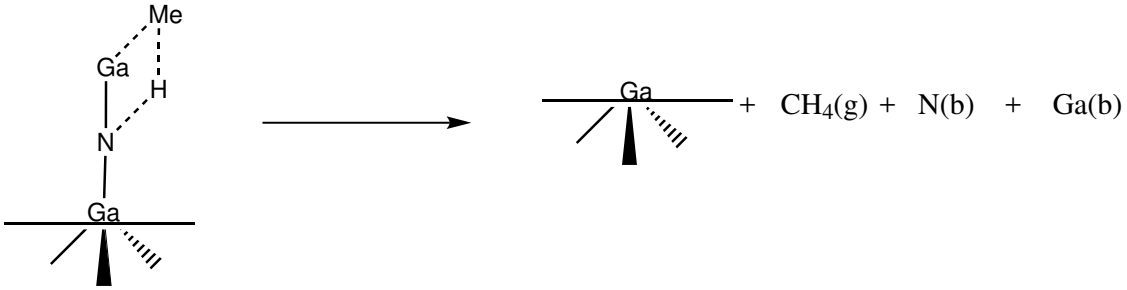

Figure 2.16: Deposition to form the bulk follwed by regeneration of Ga surface

Table 2.2: Reaction summary for GaN CVD

Reaction	Rate ($s^{-1}m^{-2}$)
$GaMe_3$ (g) + NH_3 (g) $\longrightarrow$ Me_3GaNH_3 (g)	f_0
Me_3GaNH_3 (g) $\rightleftharpoons$ $Me_3GaNH_3{}^*$ (g)	$(1/\epsilon)g_0$
$Me_3GaNH_3{}^*$ (g) $\longrightarrow$ Me_2GaNH_2 (g) + CH_4 (g)	f_1
$3Me_2GaNH_2$ (g) $\rightleftharpoons$ $(Me_2GaNH_2)_3$ (g)	$(1/\epsilon)g_1$
Me_2GaNH_2 (g) + 2S + Ga $\rightleftharpoons$ Me_2GaNH_2Ga	f_2
Me_2GaNH_2Ga $\rightleftharpoons$ $Me_2GaNH_2Ga^*$	$(1/\epsilon)g_2$
$Me_2GaNH_2Ga^*$ $\longrightarrow$ MeGaNHGa + S + CH_4 (g)	f_3
MeGaNHGa $\rightleftharpoons$ $MeGaNHGa^*$	$(1/\epsilon)g_3$
$MeGaNHGa^*$ $\longrightarrow$ Ga (b) + N (b) + CH_4 (g) + Ga + S	f_4

Chapter 3: Reaction Network Analysis: Reaction Factorization Approach

3.1 Overview

The use of mathematical analysis of chemical reaction dynamics to generate reduced order models is quite common in homogeneous systems. However, it is less common in heterogeneous systems, especially in thin-film processing. We in our group have developed a reaction factorization approach that consists of a set of Ordinary Differential Equations (ODE's) which can be factored to decouple the reaction terms [Remmers et al., 2015]. Once the reaction terms are successfully decoupled we find a set of reaction-independent modes reflecting the conserved quantities of the process with a further elimination of the dynamic modes.

In this chapter, we will apply the reaction factorization approach to the system of differential equations derived from the two reaction network models for GaAs and GaN presented in previous chapter to eliminate the redundant dynamic modes and investigate the resulting invariants.

3.2 Reaction factorization for ALD of GaAs

If we take a look at the reaction network model for GaAs which we proposed in the previous chapter we find that the initial set of reactions correspond to the first half cycle. There is the adsorption of the TMGa precursor which is a net forward rate (f_0) to produce the surface adduct. During the (1-2) H-transfer we have the formation of a critical complex. It is important to note here that while Conventional Transition State Theory (CTST) dictates this process to be an equillibrium reaction, we define it as net forward reaction rate ($(1/\epsilon)g_0$), where ϵ is the relaxation time constant for the purpose of formulating the species balances that follow.

Defining the other reaction rates in the same way and following the approach of Adomaitis et al [Adomaitis, 2016b] if we try to identify the number of species described we have $S = \{AsH_2, GaMe_3(g), AsH_2GaMe_3....\}$ which has fourteen species including the surface site defined in the previous chapter. We also have three phases with the volume of the gas phase in ϕ_0 nm^{-3}, the surface phase in ϕ_1 nm^{-2} and the bulk film phase, where the bulk phase in considered similar to the surface phase. Also, we can extract four species namely Ga, As, C and H from the reaction system defined. Using the species term S, the number of phases as two and also the surface

area term ϕ_1 we write fourteen species differential equation balance as,

$$\frac{d\mathbf{m}}{dt} = \frac{\phi_1}{\epsilon}\mathbf{P}\begin{bmatrix} g_0 \\ g_1 \\ g_2 \end{bmatrix} + \phi_1\mathbf{Q}\begin{bmatrix} f_0 \\ f_1 \\ f_2 \\ f_3 \\ f_4 \end{bmatrix} \tag{3.1}$$

As shown by [Remmers et al., 2015] and [Adomaitis, 2016b] we can write the stoichiometric arrays **P** and **Q** in the form of Equation 3.4. However, given the underlying assumptions of the CTST that the transition complexes are in equilibrium, the true solution to the Equation 3.1 is found by multiplying it by ϵ and $\epsilon \to 0$. As shown by [Adomaitis, 2016b] and [Daoutidis, 2015] this becomes an example of a Singularly Perturbed System (STS) in its non standard form. Transforming this equation using the reaction factorization procedure suggested by [Adomaitis, 2016b] we can combine the array **P** and **Q** and also g, f so that they can represented in the form of Equation 3.3 which will eventually result in the matrix shown in Equation 3.5

The matrix in Equation 3.5 is diagonalized through the Gauss-Jordan elimination procedure in order to decouple the reactions as much as possible. Following the diagonalization procedure we end up with an upper echelon matrix. It also produces three independent Differential Algebraic Equation's (DAE's) corresponding to the three equilibrium reaction rates g_0, g_1, g_2, five DAE's in time corresponding to f_0, f_1, f_2, f_3, f_4 and six conserved quantities. We can also see that in a system where there are no competing reactions, the sum of all these different modes add up to

give the total number of species, which in this case is fourteen. The six conserved quantities are referred to as reaction invariants as their value does not change with time. The DAE's generated can be solved using standard DAE solvers such as an implicit Euler scheme which is well suited for low-dimensional system for reaction rates f_i that do not span a wide range of timescales. We can also calculate the deposition if we have the numerical values of f_i using the above mentioned solver and if we project our initial conditions onto the equilibrium (g_i) manifold as shown by [Remmers et al., 2015]. The details of the above mentioned reaction factorization is explained below in a step wise manner.

$$\frac{d\mathbf{m}}{dt} = \mathbf{Rh} \tag{3.2}$$

$$where, R = \begin{bmatrix} \mathbf{P} & \mathbf{Q} \end{bmatrix}^{14\times 8}, \mathbf{h} = \begin{bmatrix} \mathbf{g} \\ \mathbf{f} \end{bmatrix}^{8\times 1} \tag{3.3}$$

$$P = \begin{bmatrix} 0 & 0 & 0 \\ 0 & 0 & 0 \\ 0 & 0 & 0 \\ -1 & 0 & 0 \\ 1 & 0 & 0 \\ 0 & -1 & 0 \\ 0 & 1 & 0 \\ 0 & 0 & 0 \\ 0 & 0 & 0 \\ 0 & 0 & 0 \\ 0 & 0 & 0 \\ 0 & 0 & -1 \\ 0 & 0 & 1 \\ 0 & 0 & 0 \end{bmatrix} \quad Q = \begin{bmatrix} -1 & 0 & 0 & 0 & 1 \\ -1 & 0 & 0 & 0 & 0 \\ -3 & 1 & 1 & 0 & 1 \\ 1 & 0 & 0 & 0 & 0 \\ 0 & -1 & 0 & 0 & 0 \\ 0 & 1 & 0 & 0 & 0 \\ 0 & 0 & -1 & 0 & 0 \\ 0 & 1 & 1 & 0 & 1 \\ 0 & 0 & 1 & 0 & 0 \\ 0 & 0 & 1 & -1 & 0 \\ 0 & 0 & 0 & -1 & 0 \\ 0 & 0 & 0 & 1 & 0 \\ 0 & 0 & 0 & 0 & -1 \\ 0 & 0 & 0 & 0 & 1 \end{bmatrix} \tag{3.4}$$

$$\frac{d}{dt}\begin{bmatrix} AsH_2 \\ GaMe_3(g) \\ AsH_2GaMe_3 \\ AsH_2GaMe_3{}^* \\ AsHGaMe_2 \\ AsHGaMe_2{}^* \\ Ga(b) \\ S \\ As(b) \\ CH_4(g) \\ GaMe \\ AsH_3(g) \\ GaMeAsH_3 \\ GaMeAsH_3{}^* \end{bmatrix} = \begin{bmatrix} 0 & 0 & 0 & -1 & 0 & 0 & 0 & 1 \\ 0 & 0 & 0 & -1 & 0 & 0 & 0 & 0 \\ -1 & 0 & 0 & 1 & 0 & 0 & 0 & 0 \\ 1 & 0 & 0 & 0 & -1 & 0 & 0 & 0 \\ 0 & -1 & 0 & 0 & 1 & 0 & 0 & 0 \\ 0 & 1 & 0 & 0 & 0 & -1 & 0 & 0 \\ 0 & 0 & 0 & 0 & 0 & 0 & 0 & 1 \\ 0 & 0 & 0 & -3 & 1 & 1 & 0 & 1 \\ 0 & 0 & 0 & 0 & 0 & 1 & 0 & 0 \\ 0 & 0 & 0 & 0 & 1 & 1 & 0 & 1 \\ 0 & 0 & 0 & 0 & 0 & 1 & -1 & 0 \\ 0 & 0 & 0 & 0 & 0 & 0 & -1 & 0 \\ 0 & 0 & -1 & 0 & 0 & 0 & 1 & 0 \\ 0 & 0 & 1 & 0 & 0 & 0 & 0 & -1 \end{bmatrix} \begin{bmatrix} (1/\epsilon)g_0 \\ (1/\epsilon)g_1 \\ (1/\epsilon)g_2 \\ f_0 \\ f_1 \\ f_2 \\ f_3 \\ f_4 \end{bmatrix} \tag{3.5}$$

DAE's corresponding to $\mathbf{g}_i$

$$\frac{d}{dt}[AsH_2GaMe_3 + GaMe_3(g)] = -(1/\epsilon)g_0 \tag{3.6}$$

$$\frac{d}{dt}[AsH_2GaMe_3 + AsH_2GaMe_3{}^* + AsHGaMe_2 + GaMe_3(g)] = -(1/\epsilon)g_1 \tag{3.7}$$

$$\frac{d}{dt}[-GaMeAsH_3{}^* - AsH_2 + GaMe_3(g)] = -(1/\epsilon)g_2 \tag{3.8}$$

DAE's corresponding to $\mathbf{f}_i$

$$\frac{d}{dt}[GaMe_3(g)] = f_0 \tag{3.9}$$

$$\frac{d}{dt}[-AsH_2GaMe_3 - AsH_2GaMe_3{}^* - GaMe_3(g) = f_1 \tag{3.10}$$

$$\frac{d}{dt}[AsH_2GaMe_3 + AsH_2GaMe_3{}^* + AsHGaMe_2 + AsHGaMe_2{}^*$$

$$+ GaMe_3(g)] = -f_2 \tag{3.11}$$

$$\frac{d}{dt}[GaMeAsH_3 + GaMeAsH_3{}^* + AsH_2 - GaMe_3(g) = f_3 \tag{3.12}$$

$$\frac{d}{dt}[-AsH_2 + GaMe_3(g) = -f_4 \tag{3.13}$$

$$\tag{3.14}$$

Reaction invariants

$$2AsH_2GaMe_3 + 2AsH_2GaMe_3{}^* + AsHGaMe_2 + AsHGaMe_2{}^*$$

$$- AsH_2 + S = w_0 \tag{3.15}$$

$$2AsH_2GaMe_3 + 2AsH_2GaMe_3{}^* + AsHGaMe_2 + AsHGaMe_2{}^*$$

$$- AsH_2 + 3GaMe_3(g) + CH_4(g) = w_1 \tag{3.16}$$

$$AsH_2GaMe_3 + AsH_2GaMe_3{}^* + AsHGaMe_2 + AsHGaMe_2{}^*$$

$$+ GaMe_3(g) + As(b) = w_2 \tag{3.17}$$

$$AsH_2GaMe_3 + AsH_2GaMe_3{}^* + AsHGaMe_2 + AsHGaMe_2{}^* + GaMeAsH_3$$

$$+ GaMeAsH_3{}^* + AsH_2 + GaMe = w_3 \tag{3.18}$$

$$GaMeAsH_3 + GaMeAsH_3{}^* + AsH_2 - GaMe_3(g) + AsH_3(g) = w_4 \tag{3.19}$$

$$- AsH_2 + GaMe_3(g) + Ga(b) = w_5 \tag{3.20}$$

3.3 Reaction factorization for CVD of GaN

We apply the same factorization techniques for GaAs ALD on to our GaN CVD system to find our reaction variants and invariants. We again determine our finite reaction rates and also write our eqiulibrium rates as finite using ϵ. Representing this deposition model in the form of Equation 3.3 we find :

$$\frac{d}{dt}\begin{bmatrix} GaMe_3(g) \\ NH_3(g) \\ Me_3GaNH_3 \\ {Me_3GaNH_3}^* \\ Me_2GaNH_2 \\ (Me_2GaNH_2)_3 \\ CH_4(g) \\ S \\ Ga \\ Me_2GaNH_2Ga \\ Me_2GaNH_2Ga^* \\ MeGaNHGa \\ MeGaNHGa^* \\ Ga(b) \\ N(b) \end{bmatrix} = \begin{bmatrix} 0 & 0 & 0 & 0 & -1 & 0 & 0 & 0 & 0 \\ 0 & 0 & 0 & 0 & -1 & 0 & 0 & 0 & 0 \\ -1 & 0 & 0 & 0 & 1 & 0 & 0 & 0 & 0 \\ 1 & 0 & 0 & 0 & 0 & -1 & 0 & 0 & 0 \\ 0 & -3 & 0 & 0 & 0 & 1 & -1 & 0 & 0 \\ 0 & 1 & 0 & 0 & 0 & 0 & 0 & 0 & 0 \\ 0 & 0 & 0 & 0 & 0 & 1 & 0 & 1 & 1 \\ 0 & 0 & 0 & 0 & 0 & 0 & -2 & 1 & 1 \\ 0 & 0 & 0 & 0 & 0 & 0 & -1 & 0 & 1 \\ 0 & 0 & -1 & 0 & 0 & 0 & 1 & 0 & 0 \\ 0 & 0 & 1 & 0 & 0 & 0 & 0 & -1 & 0 \\ 0 & 0 & 0 & -1 & 0 & 0 & 0 & 1 & 0 \\ 0 & 0 & 0 & 1 & 0 & 0 & 0 & 0 & -1 \\ 0 & 0 & 0 & 0 & 0 & 0 & 0 & 0 & 1 \\ 0 & 0 & 0 & 0 & 0 & 0 & 0 & 0 & 1 \end{bmatrix} \begin{bmatrix} (1/\epsilon)g_0 \\ (1/\epsilon)g_1 \\ (1/\epsilon)g_2 \\ (1/\epsilon)g_3 \\ f_0 \\ f_1 \\ f_2 \\ f_3 \\ f_4 \end{bmatrix} \tag{3.21}$$

On performing the Gauss-Jordan elimination we obtain four DAE's for g_0, g_1, g_2, g_3, five DAE's in time corresponding to f_0, f_1, f_2, f_3, f_4 and six conserved quantities.

DAE's corresponding to $\mathbf{g}_i$

$$\frac{d}{dt}[Me_3GaNH_3(g) + GaMe_3(g)] = -(1/\epsilon)g_0 \tag{3.22}$$

$$\frac{d}{dt}[(Me_2GaNH_2)_3] = g_1 \tag{3.23}$$

$$\frac{d}{dt}[Me_3GaNH_3(g) + Me_3GaNH_3{}^*(g) + Me_2GaNH_2(g) + 3(Me_2GaNH_2)_3(g)$$

$$+ Me_2GaNH_2Ga + GaMe_3(g)] = -(1/\epsilon)g_2 \tag{3.24}$$

$$\frac{d}{dt}[Me_3GaNH_3(g) + Me_3GaNH_3{}^*(g) + Me_2GaNH_2(g) + 3(Me_2GaNH_2)_3(g)$$

$$+ Me_2GaNH_2Ga + Me_2GaNH_2Ga^* + MeGaNHGa + GaMe_3(g)] = -(1/\epsilon)g_3$$

$$\tag{3.25}$$

DAE's corresponding to $\mathbf{f}_i$

$$\frac{d}{dt}[-GaMe_3(g)] = f_0 \tag{3.26}$$

$$\frac{d}{dt}[-Me_3GaNH_3(g) - Me_3GaNH_3{}^*(g) - GaMe_3(g)] = f_1 \tag{3.27}$$

$$\frac{d}{dt}[-Me_3GaNH_3(g) - Me_3GaNH_3{}^*(g) - GaMe_3(g) - Me_2GaNH_2(g) - GaMe_3(g)$$

$$- 3(Me_2GaNH_2)_3(g)] = f_2 \tag{3.28}$$

$$\frac{d}{dt}[-Me_3GaNH_3(g) - Me_3GaNH_3{}^*(g) - GaMe_3(g) - Me_2GaNH_2(g) - GaMe_3(g)$$

$$- 3(Me_2GaNH_2)_3(g) - Me_2GaNH_2Ga - Me_2GaNH_2Ga^*] = f_3 \tag{3.29}$$

$$\frac{d}{dt}[-Me_3GaNH_3(g) - Me_3GaNH_3{}^*(g) - GaMe_3(g) - Me_2GaNH_2(g) - GaMe_3(g)$$

$$- 3(Me_2GaNH_2)_3(g) - Me_2GaNH_2Ga - Me_2GaNH_2Ga^* - MeGaNHGa$$

$$- MeGaNHGa^*] = f_4 \tag{3.30}$$

Reaction invariants

$$-GaMe_3(g) + NH_3(g) = z_0 \tag{3.31}$$

$$3Me_3GaNH_3(g) + 3Me_3GaNH_3{}^*(g) + 2Me_2GaNH_2(g) + 6(Me_2GaNH_2)_3(g)$$
$$+ 2Me_2GaNH_2Ga + 2Me_2GaNH_2Ga^* + MeGaNHGa + MeGaNHGa^*$$
$$+ 3GaMe_3(g) + CH_4(g) = z_1 \tag{3.32}$$

$$2Me_2GaNH_2Ga + 2Me_2GaNH_2Ga^* + MeGaNHGa$$
$$+ MeGaNHGa^* + S = z_2 \tag{3.33}$$

$$2Me_2GaNH_2Ga + 2Me_2GaNH_2Ga^* + MeGaNHGa$$
$$+ MeGaNHGa^* + Ga = z_3 \tag{3.34}$$

$$Me_3GaNH_3(g) + Me_3GaNH_3{}^*(g) + Me_2GaNH_2(g) + 3(Me_2GaNH_2)_3(g)$$
$$+ Me_2GaNH_2Ga + Me_2GaNH_2Ga^* + MeGaNHGa + MeGaNHGa^*$$
$$+ GaMe_3(g) + Ga(b) = z_4 \tag{3.35}$$

$$Me_3GaNH_3(g) + Me_3GaNH_3{}^*(g) + Me_2GaNH_2(g) + 3(Me_2GaNH_2)_3(g)$$
$$+ Me_2GaNH_2Ga + Me_2GaNH_2Ga^* + MeGaNHGa + MeGaNHGa^*$$
$$+ GaMe_3(g) + N(b) = z_5 \tag{3.36}$$

In both cases we can see from the DAE's corresponding to g_i's that if we have $\epsilon \to 0$, $g_i = 0$. Thus the reaction diagonalization procedure determines if the pseudo-equilibrium relationships can be solved independently at all times during the simulation thereby confirming that the reaction time scales can be separated when $\epsilon \to 0$. Thus, by using the Gaussian factorization approach we were successful in decoupling the reaction terms and also identifying the conserved quantities in

both the ALD and CVD systems. We also have the reaction variants which are the DAE's corresponding to the f_i which can be used to predict gpc. While we have six conserved species in each case, the Equations 3.31-3.36 and Equations 3.15-3.20 reveals very little with respect to the physical meaning of these quantities. Thus, the challenge lies in identifying what the six conserved modes physically signify.

Chapter 4: Reaction Network Analysis: Species-Reaction Graph Appraoch

4.1 Introduction

The idea of Species-Reaction (S-R) graph stems from [Craciun and Feinberg, 2006] who used it to identify multiple equilibria in complex chemical reaction networks. The S-R graph is similar to the network of reactions usually depicted in complex biological networks. The inspection of these S-R graphs often tells the essence of the reaction and process under study. This idea was further extended by Adomaitis et al by applying it to thin film deposition systems to understand the extraction of invariants from reaction networks. His paper [Adomaitis, 2017] explains the rules involved in extracting the invariants from the graph. In this chapter we define prototype systems to explain the S-R graph and the rules involved in identifying invariants.

4.2 The Species-Reaction Graph

The S-R graph is a very simple and easy way of visualizing a complex reaction mechanism. Chemical species and reactions form the nodes of the graph. A species

in the reaction is represented by a circle around its name and a reaction rate of any process is given inside a square box. Among the rates we find 'f' and 'g' with subscripts for naming the subsequent processes where 'f' denotes finite forward rate while 'g' represents equilibrium reaction. We have edges connecting the species and reactions. The coefficeints on these edges represents the stoichiometry. A negative sign on these coefficients indicates a reactant and positive sign indicates product.

A simple prototype system is discussed to explain this idea. Assume we have three species A, B and C. 'A' is in the gas phase which is adsorbed onto species 'B' on the surface to give 'AB' which gives the bulk phase 'C' via a transition state 'AB*'. Along with the bulk phase, two moles of a gas 'D' is also generated. This process is summarized the Table 4.1

Table 4.1: Reaction summary for the prototype system

Reaction	Rate ($s^{-1}m^{-2}$)
$\lvert V_{R0}\rvert$A (g)+$\lvert V_{Q0}\rvert$B $\longrightarrow$ $\lvert V_{P0}\rvert$AB	f_0
$\lvert V_{R1}\rvert$AB $\rightleftharpoons$ $\lvert V_{P1}\rvert$AB*	$(1/\epsilon)g_0$
$\lvert V_{R2}\rvert$AB* $\longrightarrow$ $\lvert V_{Q1}\rvert$C (b) + $\lvert V_{P2}\rvert$D (g)	f_1

Where, $V_{R0} = V_{Q0} = V_{R1} = V_{R2} = -1$, $V_{P0} = V_{P1} = V_{Q1} = 1$ and $V_{P2} = 2$

This reaction can be represented as a S-R graph as shown in Figure 4.1. We can see that one mole of 'A' is consumed which is denoted by the coeffcient '-1' on the line connecting 'A' and reaction rate 'f_0'. We can also see that there is the surface species 'B' also connecting to f_0 showing that one mole of even that is consumed to result in species 'AB'. Since 'AB' is a product of this reaction we find a coefficient

'+1' on the edge connecting 'f_0' and 'AB'. It is also important to note that in the final reaction where two moles of the gas species 'D' is formed we have '2' on the edge connecting 'f_1' and 'D(g)'. Thus, the S-R graph is self explanatory about the reactions and their stoichiometry. The next important thing the graph explains is the invariants in the system. However, given the complexity of the prototype graph we turn to examining its sub graphs to extract the invariants.

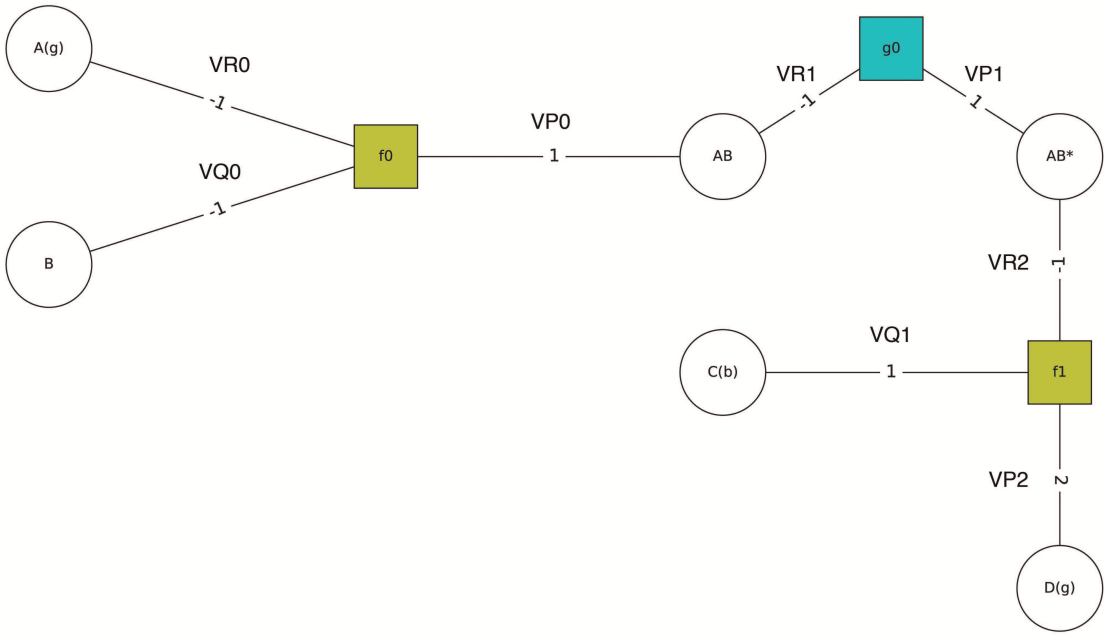

Figure 4.1: The S-R graph for the prototype system

4.3 Rules to extract invariants from the S-R graph

Due to the complexity of the S-R graph induced by the reaction networks we need to take a closer look at the subgraphs in the system to understand their connections to the reaction invariants. We look at the possible cases that are generally

encountered in a typical reaction network.

4.3.1 Terminal species to Terminal species

When we are tracing from one terminal species to another terminal species we can derive a rule to identify conservation. Let us use the system defined in the earlier section Figure 4.1. Every S-R graph which has only chemical species as terminal nodes and not rate processes is a closed system. Thus, we can expect at least one invariant in the system. We see that while tracing from species 'A' to species 'D' if we have alternating signs then we can claim that :

$$A + \frac{|V_{R0}|}{|V_{P0}|}\left[AB + \frac{|V_{R1}|}{|V_{P1}|}\left[AB^* + \frac{|V_{R2}|}{|V_{P2}|}D\right]\right] = invariant \tag{4.1}$$

$$2A + 2AB + 2AB^* + D = w_0 \tag{4.2}$$

The idea of alternating signs is nothing but a reflection of the rates from the factorization matrix. In order to understand this idea better let us start with the matrix which we can write based on 3.3. We have,

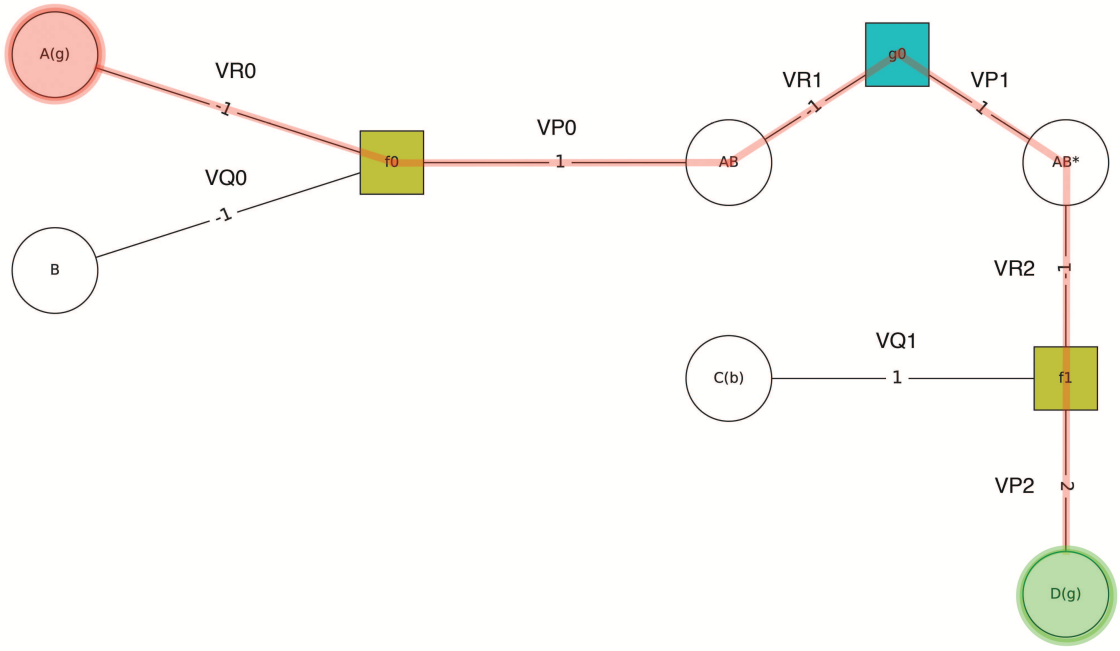

Figure 4.2: An example showing invariant in a S-R graph

$$\frac{d}{dt}\begin{bmatrix} A \\ B \\ AB \\ AB^* \\ C \\ D \end{bmatrix} = \begin{bmatrix} 0 & -|V_{R0}| & 0 \\ 0 & -|V_{Q0}| & 0 \\ -|V_{R1}| & |V_{P0}| & 0 \\ |V_{P1}| & 0 & -|V_{R2}| \\ 0 & 0 & |V_{Q1}| \\ 0 & 0 & |V_{P2}| \end{bmatrix} \begin{bmatrix} g_0 \\ f_0 \\ f_1 \end{bmatrix} \tag{4.3}$$

If we now follow the Gauss-Jordan elimination procedure to obtain a upper-echelon matrix we find, at every reaction node we will add and subtract reaction rates which will result in only the rates of the terminal species being left out. If all the rates cancel out then instead of a terminal to terminal connection we will have a circular loop as will be discussed later. Also, we have a total of three independent

invariants that can be derived from the S-R graph. It is important to note that, if we perform the Gauss-elimination for the above reaction network we will find that the network has three invariants which shows that both analysis are in agreement.

To find out the other two invariants we can trace from the terminal species 'B' to terminal species 'C' to obtain one of them. Again it is important to note that we are looking at routes where is there is sign change when moving from one edge to another as explained earlier.

$$B + \frac{|V_{Q0}|}{|V_{P0}|}\left[AB + \frac{|V_{R1}|}{|V_{P1}|}\left[AB^* + \frac{|V_{R2}|}{|V_{Q1}|}C\right]\right] = invariant \tag{4.4}$$

$$B + AB + AB^* + C = w_1 \tag{4.5}$$

and the last invariant will be,

$$A + \frac{|V_{R0}|}{|V_{P0}|}\left[AB + \frac{|V_{R1}|}{|V_{P1}|}\left[AB^* + \frac{|V_{R2}|}{|V_{Q1}|}C\right]\right] = invariant \tag{4.6}$$

$$A + AB + AB^* + C = w_2 \tag{4.7}$$

Thus any combination of these can also be traced from one terminal species to another.

4.3.2 Reaction Branches

To understand the invaraints that can be extracted from a reaction branch we define a very simple reaction scheme.

$$OH \ + \ CH_3A \ (g) \xrightarrow{f_0} OA \ + \ CH_4 \ (g)$$

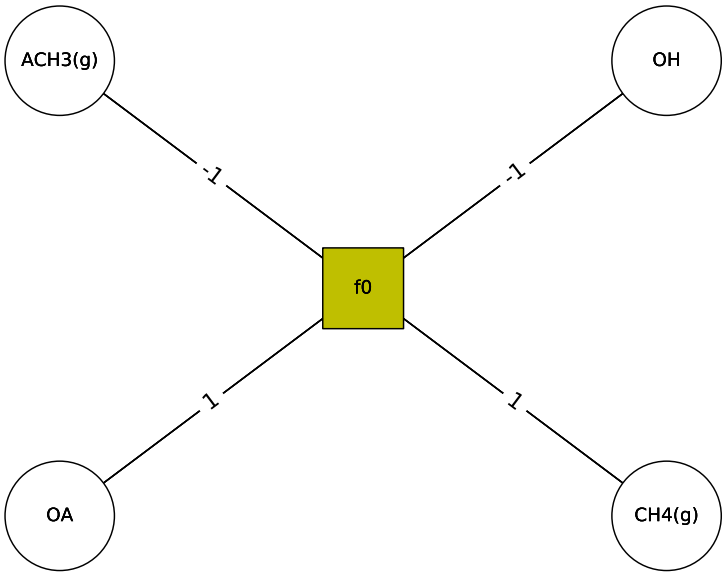

Figure 4.3: An example to understand the reaction branching rule

For simplicity in dealing with our invariant relation and also because of the fact that CH_3 is not separated through the course of this reaction we say CH_3 = Me. So, we have a total of four species represented as Me, H, O and A. By using the terminal species to terminal species rule we can find our four invariants from Figure 4.4.

$$OH + OA = constant = a \tag{4.8}$$

$$OH + MeH = constant = b \tag{4.9}$$

$$MeA + OA = constant = c \tag{4.10}$$

$$MeA + MeH = constant = b + c - a \tag{4.11}$$

These are thus equations derived when the paths pass through the reaction. However, there are also paths which bypass the reaction. For instance,

$$MeA - OH = c - a$$

$$OA - MeH = a - b$$

which are just linear combinations of (a-d) passing through the reactions. It is important to note at this point that negative quantities in invariants like in Equation 3.20 originate from paths that pass that bypass the reaction complexes. However, to generate physically meaningful invariants we focus on generating invariants corresponding to the paths that pass through the reaction and thus we look for paths where we have stoichiometric coefficient changing sign between the incoming and outgoing edge. These first three Equations 4.8, 4.9, 4.10 are linearly independent. To understand what a combination of these mean we take a closer look at Equation 4.11, which has all the terms corresponding to 'Me' to account for the conservation of 'Me'.

$$MeA + MeH = constant = b + c - a = w_0$$

It is evident that Equation 4.8 represents that conservation of sepcies 'O' ,Equation 4.9 represents the conservation of species 'H'.and Equation 4.10 represents the conservation of species 'A'.

$$OH + OA = b + c - a = w_1$$

$$MeA + OA = c = w_2$$

$$OH + MeH = c = w_3$$

where MeH is nothing but CH_4.

We can try to understand the above in terms of matrices. To do that we first create an atomic balance array 'A'.

	OH	MeA	OA	MeH	
Me	0	1	0	1	w_0
O	1	0	1	0	w_1
A	0	1	1	0	w_2
H	1	0	0	1	w_3

The atomic balance array gives us an understanding of the elemental balance that is necessary. We need check if the atomic balance array satisfies the coefficients or weights of these edges that we find in the S-R graph. Since we are looking for invariants, we can solve the equation $A.X = 0$, where the 'X' matrix contains the set of all null space solutions for the equation. This is called the Kernel of A. We can also find the dimension of the Kernel of A which will give us the nullity of the matrix A.

$nullity = no : ofcolumns - rank(A) = 1$

Where A = Atomic balance array We can solve for X which gives us the,

$Kernel = [-1, -1, 1, 1]^T$

which is nothing but vector of the stoichiometric coefficients of the reaction system.

Another perspective of looking at this is in the form of logical OR gate. We can say that while performing Gauss-elimination for this system a combination that involves just one operation with one of the other rows of the matrix will result in a row filled with zero's. Thus, we just need one OR the other rows in the matrix to add up to eliminate this row. We can also see that it is just an extension of the species branching rule that helps generate multiple invariants in Equation 4.1.

4.3.3 Species Branches

In the first rule we explained about reaction branches, but it is sometimes possible that two independent reactions can involve the same reactant for example, a single species undergoing ligand substitution and thermal decomposition at the same time. The selectivity of such a reaction will be determined by kinetics based on f_0, f_1 values. In such cases it is important to define another rule that can explain the invariant in the reaction system. We again introduce a prototype systems to understand this rule.

We examine the species A and B as a combination of two molar subset quantities $A^{(1)} + A^{(2)}$ and $B^{(1)} + B^{(2)}$ respectively. if we apply the terminal to terminal species rule from A to C as well as from A to D, we find

$$A^{(1)} + B^{(1)} + C + D = constant \tag{4.12}$$

$$A^{(2)} + B^{(2)} + C + D = constant \tag{4.13}$$

therefore,

$$A + B + C + D = w_0 \tag{4.14}$$

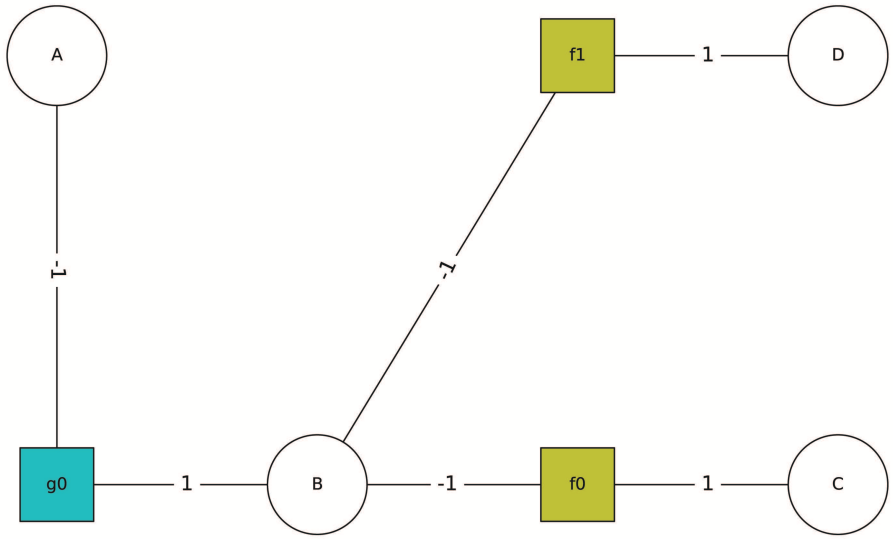

Figure 4.4: An example to understand the species branching rule

It is important to note that the species $A^{(1)}$, $A^{(2)}$, $B^{(1)}$ and $B^{(2)}$ are all artificial quantities and do not physically exist. Similarly Equations 4.12 and 4.13 are also not physically realizable invariants and the only true invariant corresponds to Equation 4.14.

4.3.4 Cycles in S-R graphs

There are cases where we have species A forming two moles of an intermediate B which forms four moles of C which in turn results in A. This system is purposefully made complicated to get a better understanding of how reaction stoichiometry is reflected in the invariant relation. It is also interesting to note that a similar system is in fact studied by Wei and Prater [Wei and Prater, 1962]. When we have networks which form a closed loop as in the case of Equation 4.15 , we can try to imagine them as linear graphs. So, we expand the closed loop to give us an open network as

shown in Figure 4.6. Again we have to keep in mind that $A^{(1)}$ and $A^{(2)}$ are artificial molar sub totals and do not exist in reality. Thus, now we can think of moving from one terminal species to another. At every reaction node we have the rate terms canceling out and since, both the terminal species add up to give A, the reaction pathway ends up forming a closed loop. So we can use the terminal species rule to write our invariant as

$$\mathrm{A} \underset{}{\overset{g_0}{\rightleftharpoons}} 2\mathrm{B} \overset{g_1}{\rightleftharpoons} 4\mathrm{C} \overset{f_0}{\rightleftharpoons} \mathrm{A} \tag{4.15}$$

$$A^{(1)} + C + 2B + 4A^{(2)} = constant \tag{4.16}$$

and from Figure 4.5 we can see that,

$$A^{(1)} + A^{(2)} = A \tag{4.17}$$

So,

$$4A + 2B + C = w_0 \tag{4.18}$$

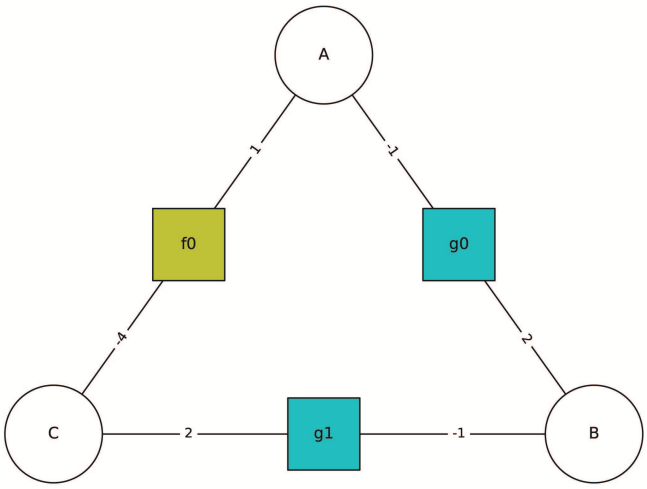

Figure 4.5: Circular loops in S-R graphs

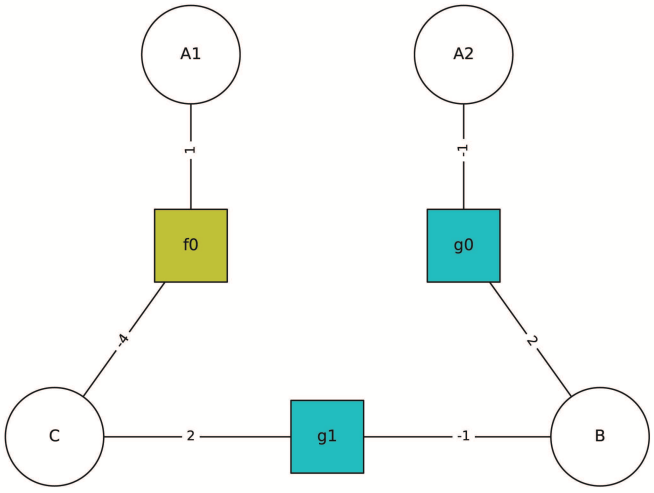

Figure 4.6: Circular loop as a linear network

Chapter 5: Species-Reaction Graphs for GaAs and GaN

After we have successfully understood the rules of extracting invariants from the S-R graph we now trace them in the network to actually identify these invariants. One of our most important reason for the representation of these networks is to simplify the process of invariant extraction, it not only saves us valuable time by skipping the Gaussian factorization approach but also helps us identify if the mechanism is viable. In this chapter we summarize our findings from the S-R graphs and show how they relate to the conserved quantities obtained from the factorization approach.

5.1 Extracting invariants from S-R graph for GaAs ALD

A S-R graph for the ALD of GaAs is shown in Figure 5.1. Our idea of understanding invariants through the S-R graph is achieved by tracing through the network. To simply this idea we start our tracing at the species which is highlighted by red and the end of the path is identified by a species highlighted by the green color. In cases where branching is involved we represent different colors to identify those multi pathways.

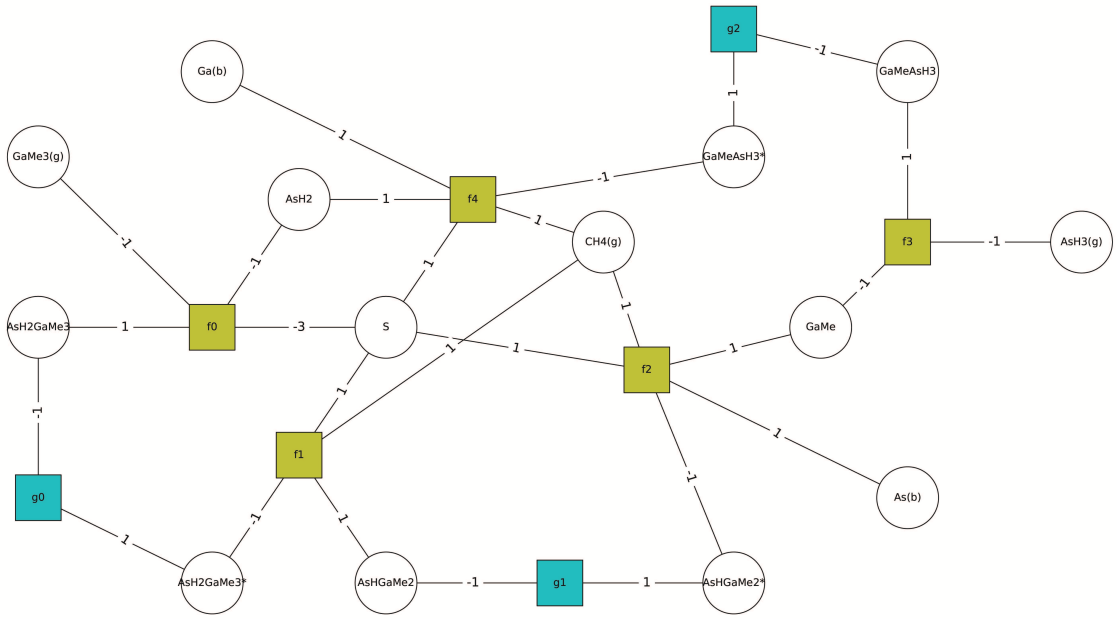

Figure 5.1: S-R graph the ALD of GaAs

5.1.1 Gallium conservation

We start our reaction path with the precursor TMGa ($GaMe_3(g)$) which is a terminal species, its adsorption on to the reactive site results in the formation of a series of surface species and their respective complexes which are traversed by our path. Finally we end up at the bulk gallium (Ga(b)) which is another terminal species. If we write this in terms of species strings we find

$$GaMe_3(g) + AsH_2GaMe_3 + AsH_2GaMe_3{}^* + AsHGaMe_2 + AsHGaMe_2{}^* + GaMe + GaMeAsH_3 + GaMeAsH_3{}^* + Ga(b) = constant$$

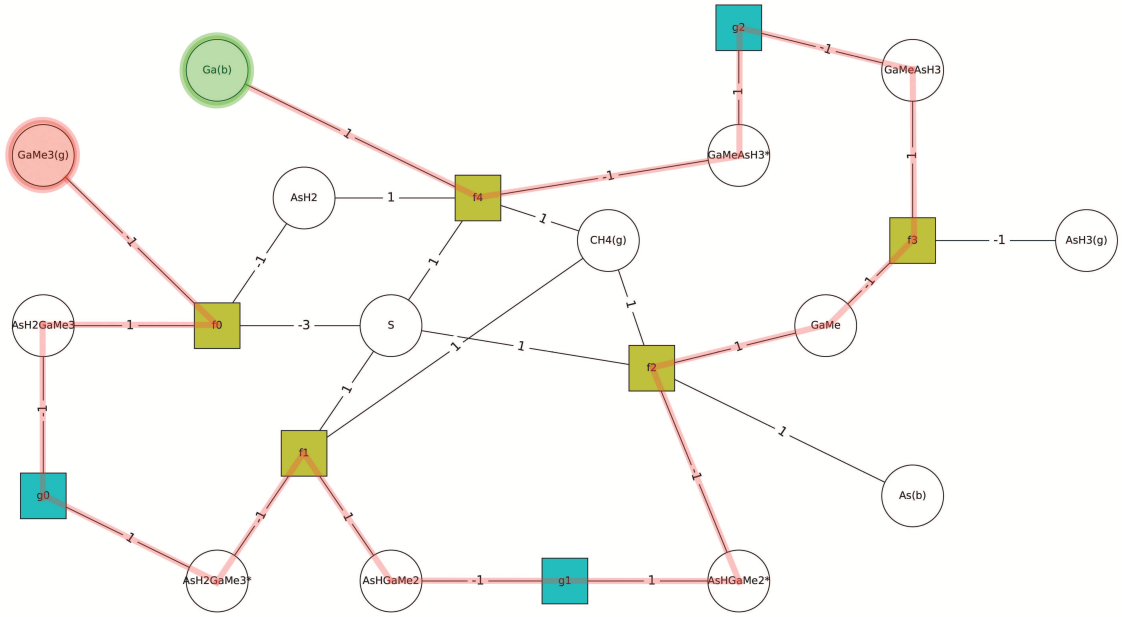

Figure 5.2: S-R graph for the conservation of gallium in GaAs ALD

5.1.2 Arsenic conservation

Arsenic conservation can be traced from its precursor arsine ($AsH_3(g)$) which is a terminal species. We can then travel through the surface species and their complexes before we end at the bulk arsenic (As(b)). If we write this in terms of species strings we find,

$$AsH_3(g) + GaMeAsH_3 + GaMeAsH_3{}^* + AsH_2 + AsH_2GaMe_3 + AsH_2GaMe_3{}^* + AsHGaMe_2 + AsHGaMe_2{}^* + As(b) = constant$$

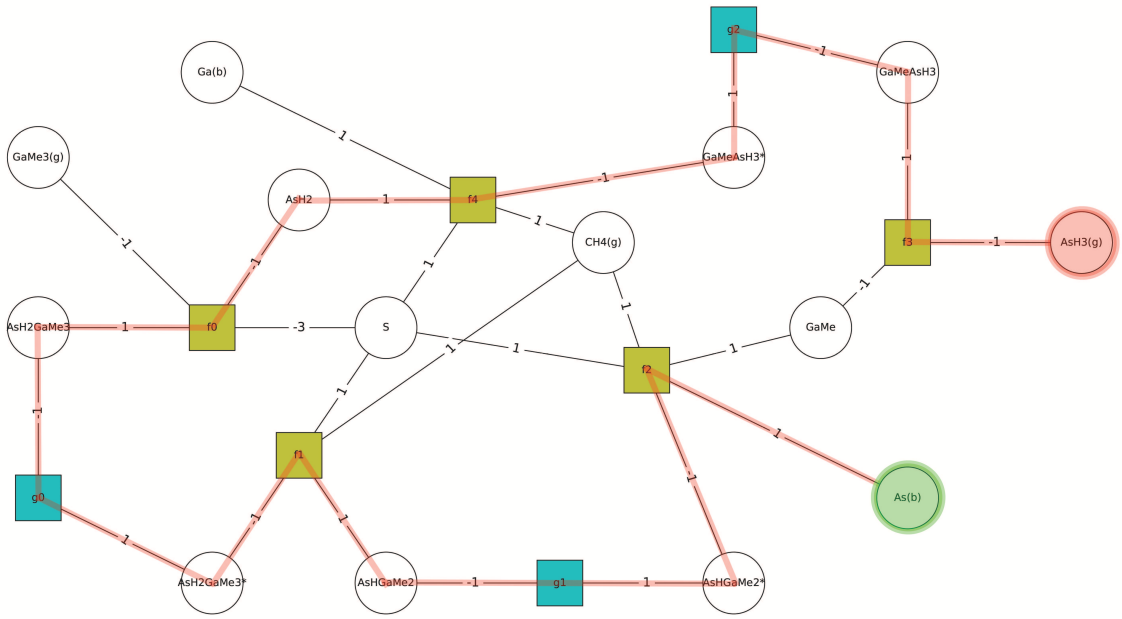

Figure 5.3: S-R graph for the conservation of arsenic in GaAs ALD

5.1.3 Methyl group conservation

Instead of looking for carbon conservation we look for methyl group conservation since 'C' is always found as CH_3 or Me. CH_4 can also be looked at as MeH. We start with the terminal species $GaMe_3(g)$ and end at the other terminal species which is CH_4. However, it is important to note that here methane terminates through three different routes and we account for all that using our reaction and species branching rule. The reaction branching at f_1, f_2 and f_4 can be understood as producing molar sub totals of CH_4 namely $CH_4^{(1)}$, $CH_4^{(2)}$, $CH_4^{(3)}$ where $CH_4 = CH_4^{(1)} + CH_4^{(2)} + CH_4^{(3)}$. It is also important to keep in mind that, as described earlier these molar partial molar quantities are not a physical quantities but rather a mathematical representation for easy interpretation of our paths. We can write

the conservation from the graph as,

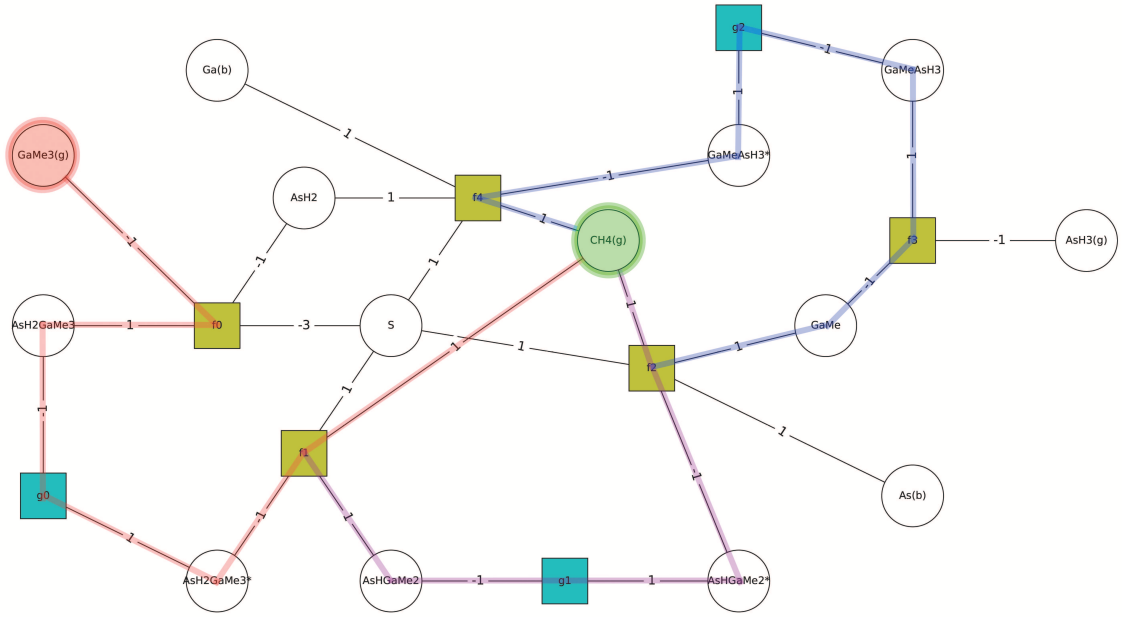

Figure 5.4: S-R graph for the conservation of methyl in GaAs ALD

$$3GaMe_3(g) + 3AsH_2GaMe_3 + 3AsH_2GaMe_3{}^* + {CH_4}^{(1)}(g) \qquad (Red \quad line)$$

$$+ 2AsHGaMe_2 + 2AsHGaMe_2{}^* + {CH_4}^{(2)}(g) \qquad (Purple \quad line)$$

$$+ GaMe + GaMeAsH_3 + GaMeAsH_3{}^* + {CH_4}^{(3)}(g) = constant \qquad (Blue \quad line)$$

5.1.4 Hydrogen transfer conservation

In the earlier invariant the idea of carbon conservation was looked from the point of view of methyl groups conservation. In the same way we can see that 'H' is also a part of this methyl groups. Thus the methyl group conservation also conserves the hydrogens that are part of them. Now we can look for species that have hydrogen's as "H" and hence we term this a hydrogen "transfer" conservation

(or H-transfer conservation) and not hydrogen conservation since we have already accounted for the conservation of methyl hydrogens. Thus we start at the precursor arsine AsH_3(g) and move through the network till we reach CH_4 which can be understood as MeH. We again have molar sub totals of CH_4 being formed at the three reaction branches f_1, f_2 and f_4. If we write them in terms of species strings we have,

$$3AsH_3(g) + 3GaMeAsH_3 + 3GaMeAsH_3{}^* + CH_4{}^{(1)} \qquad (Red \quad line)$$

$$+ 2AsH_2 + 2AsH_2GaMe_3 + 2AsH_2GaMe_3{}^* + CH_4{}^{(2)}(g) \qquad (Purple \quad line)$$

$$+ AsHGaMe_2 + AsHGaMe_2{}^* + CH_4{}^{(3)}(g) = constant \qquad (Blue \quad line)$$

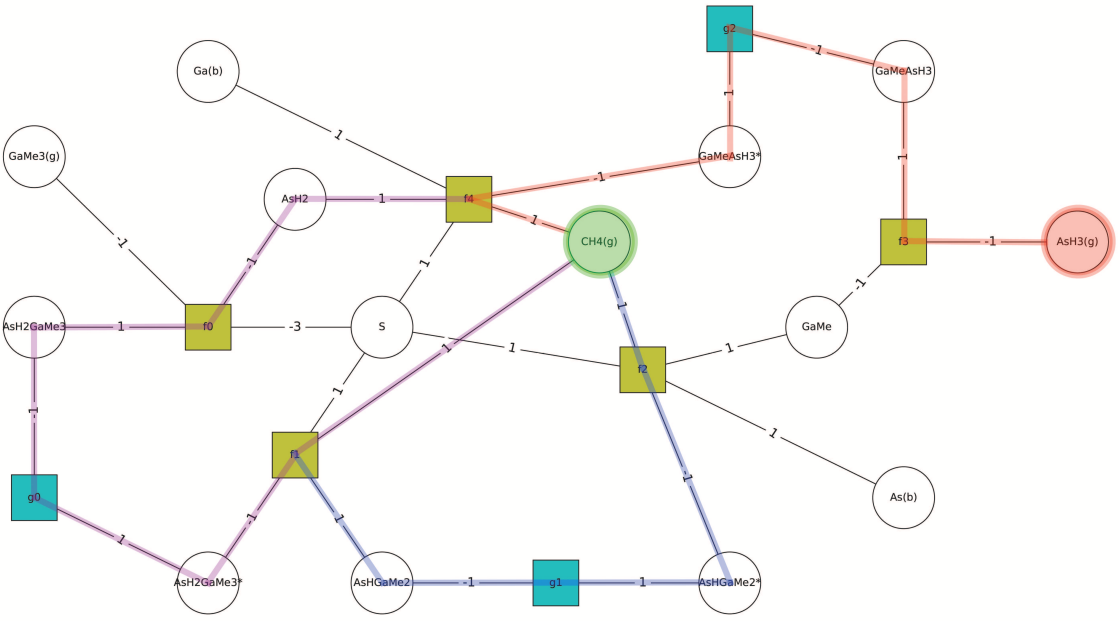

Figure 5.5: S-R graph for the conservation of hydrogen transfer in GaAs ALD

5.1.5 Reactive site conservation

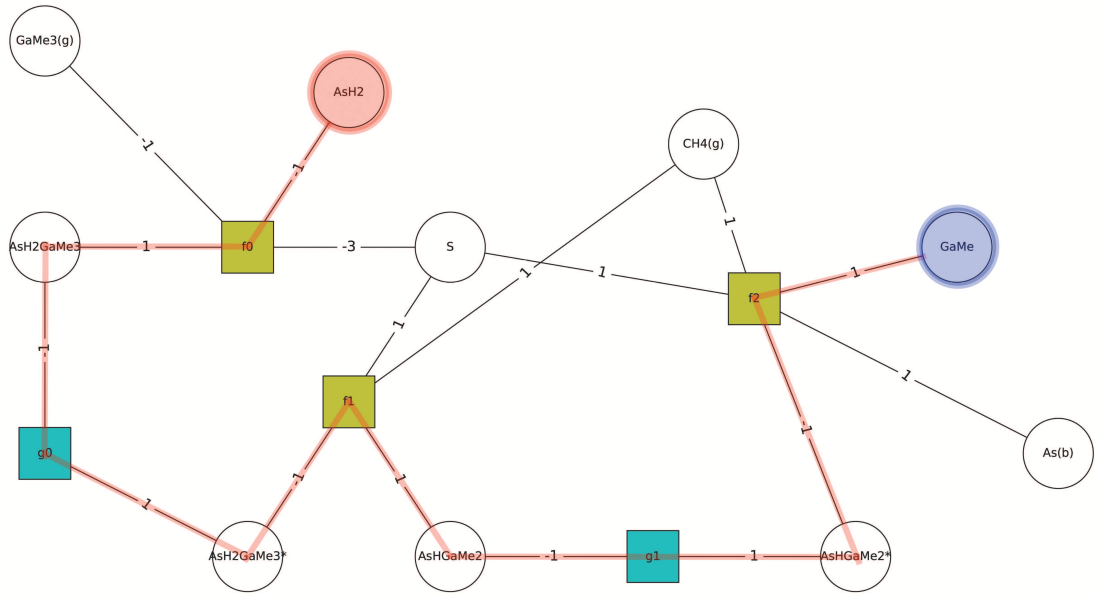

Figure 5.6: S-R graph representing the first half cycle in GaAs ALD

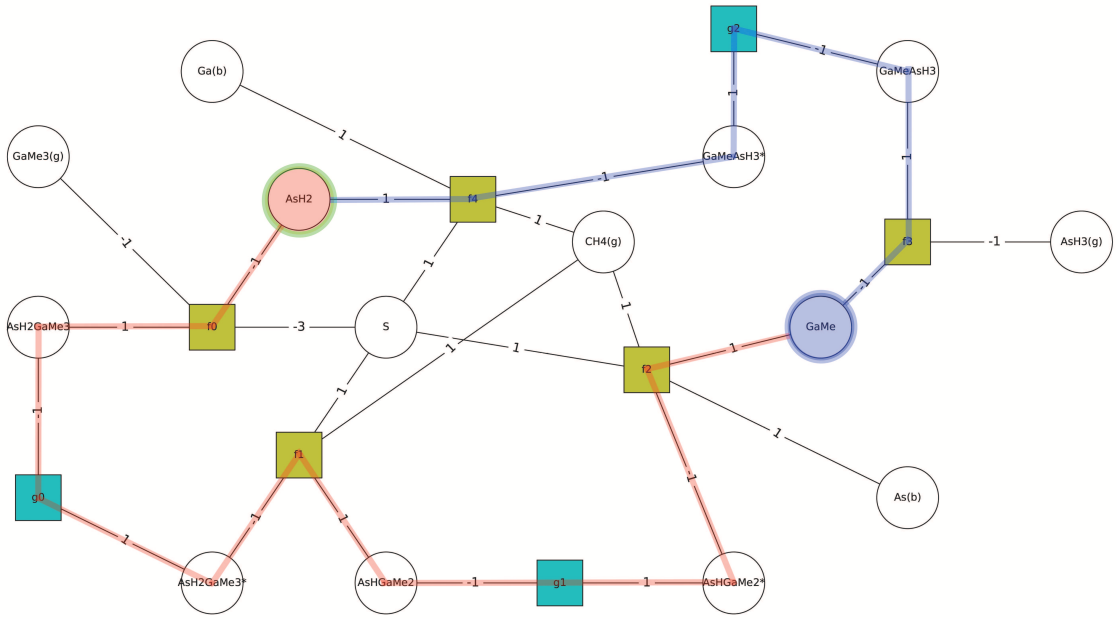

Figure 5.7: S-R graph for the conservation of reactive sites in GaAs ALD

As we stated in the first chapter one of our foremost aims is to understand ALD from the perspective of reaction networks. Our reactive site conservation proves that our reaction is a self limiting one, the most important feature of any ALD process. We can understand this by tracing the reaction network from AsH_2 which is our initial surface site for adsorption of the TMG precursor. At the end of the first half cycle we see that GaMe is generated as shown in Figure 5.6. Thus, we cannot have any further deposition of the TMGa precursor which proves the self limiting nature.

For the second half cycle, we start at GaMe and the arsine precursor gets adsorbed and then in the final step we get back our original surface site AsH. So, we have two half cycles, the end of the first half cycle shows that if there is no second precursor pulse our growth gets saturated and there is just GaMe on the surface. Once the second precursor gets adsorbed on the GaMe surface we have the completion of the entire cycle. This result shows our surface is reproducible. Thus, the existence of a circular loop for reactive site conservation is a proof that our ALD mechanism which is both self limiting and reproducible is indeed a plausible one. We also see that in the reactive site invariant equation we have all the species present on the reaction site and they add up to a give a constant value.

$$AsH_2^{(1)} + AsH_2GaMe_3 + AsH_2GaMe_3{}^* + AsHGaMe_2 + AsHGaMe_2{}^* + GaMe \quad (Redline)$$

$$+ GaMeAsH_3 + GaMeAsH_3{}^* + AsH_2^{(2)} = constant \quad (Blueline)$$

5.1.6 Surface site conservation

However, the presence of reactive site conservation alone cannot necessarily prove that its self limiting. The conservation of surface site is equally important for any ALD system. Its conservation proves that only a fractional surface is available for the adsorption process and is a key factor for its self limiting nature. For surface site conservation, we need to begin tracing our network path at 'S', three moles of which is consumed and it can be traced into three different closed cycles which generates one mole of 'S' species at the end. Each of these pathways is again represented by a different color for better understanding and can be understood as regenerating sub molar quantities of 'S'.

The first cycle represented by the red line, involves consumption of three surface site due to the adsorption of the precursor. So, during the TMGa adsorption we have both $f_2 = f_4 = 0$ corresponding to no adsorption of the arsine precursor. Once we have the completion of two stoichiometrically unsaturated cycles then we have the adsoption of the arsine precursor which eventually facilitates the regeneration of all the surface sites 'S' as shown by the blue line. Thus, $S^{(1)} + S^{(2)} + S^{(3)} + S^{(4)} = S$. By stoichiometrically unsaturated cycles we mean that only a sub-molar quantity of the total moles of surface site 'S' is regenerated at the end of the cycle. Only if all the three surface sites are regenerated can we have further adsorption of the TMGa, which shows why the presence of huge ligands play an important role in self limiting growth.

$$S^{(1)} + AsH_2GaMe_3 + AsH_2GaMe_3{}^* + S^{(2)} \qquad (Red \quad line)$$

$$+ AsHGaMe_2 + AsHGaMe_2{}^* + S^{(3)} \qquad (Purple \quad line)$$

$$+ GaMe + GaMeAsH_3 + GaMeAsH_3{}^* + S^{(4)} = constant \qquad (Blue \quad line)$$

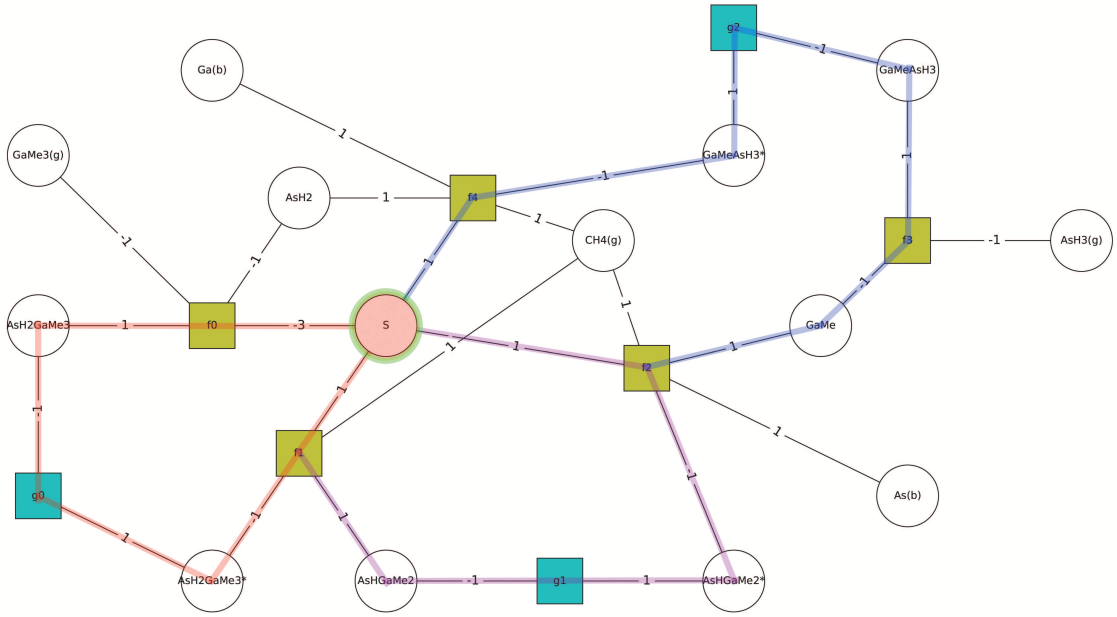

Figure 5.8: S-R Graph for the conservation of surface sites in GaAs ALD

So, out of the six invariants four of them describes species conservation which is quite straightforward. However, an indepth analysis of the other two invariants shows how they are very specific to the ALD process. At the end of each half cycle we see that the process is self limited, which means no further deposition occurs without injection of a precursor pulse. We can also see that at the end of each complete cycle we have regeneration of the original reaction site. This means that our process is reproducible which is consistent with the idea of any ALD process. The surface

site conservation invariant also shows that our process is a self-limiting one. Thus, any reaction mechanism which leads to a sub monolayer growth can be verified by understanding the steric hindrance of the ligands on the surface. For example an Alumina ALD might have a sub monolayer growth because of the presence of these surface sites, at the same time we can have more than one monolayer growth when we have enough reaction sites on the surface and also less steric hindrance from the ligands. Hence, the final two invariants clearly are characteristic to any ALD process and the presence of these two invariants verifies the possibility of a "proper" ALD.

5.2 Extracting invariants from S-R graph for GaN CVD

Before we extract the invariants of a GaN CVD from the S-R graph, it is important to understand a primary difference between ALD and CVD networks in terms of S-R graphs. In a CVD process since we have both the precursors being input into the system at the same time it becomes relatively easy to spatially separate all the chemical species based on their phases. This is clearly represented in the S-R graph for the GaN system in Figure 5.9. We can see that the reactions at f_2 and f_4 span two phases.

The formulation of invariants for a CVD system is very similar to an ALD system. Here again we have six invariants which can be derived from the S-R graphs by applying our invariant extraction rules. Also, similar to the GaAs system we represent the start of a terminal pathway by a red circle around the species and

the end by a green circle. In addition due to the presence of a reaction branch in our case, we represent one of the end points ($(Me_2GaNH_2)_3(g)$) of the reaction branch by an orange circle.

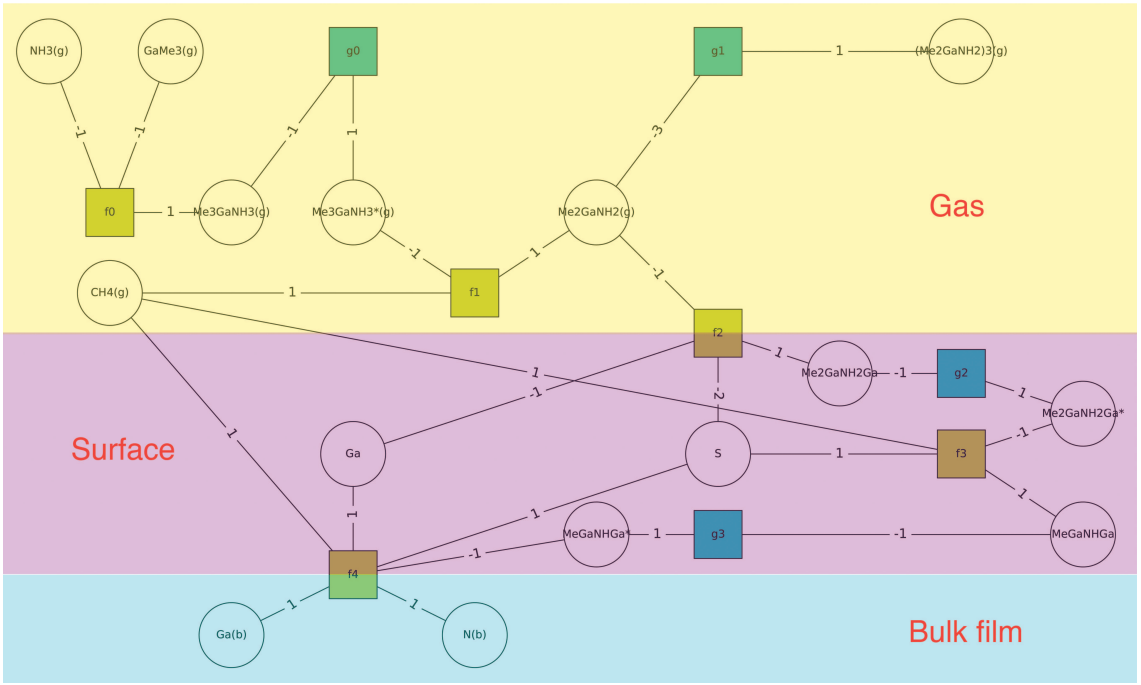

Figure 5.9: S-R graph for the CVD of GaN showing phase seperation

5.2.1 Gallium conservation

The conservation of gallium can be traced from the gas phase precursor TMGa to the bulk film phase where we have the deposited Ga. In the case of our CVD system we see that the precursor undergoes a adduct formation reaction which leads to a monomer species by the removal of a CH_4 group. At this point we have a species branching which results in the formation of a trimer. We apply the species branching rule to account for trimer species by representing it as an orange circle connected by a red line. We see that in order to account for the gallium surface site and also

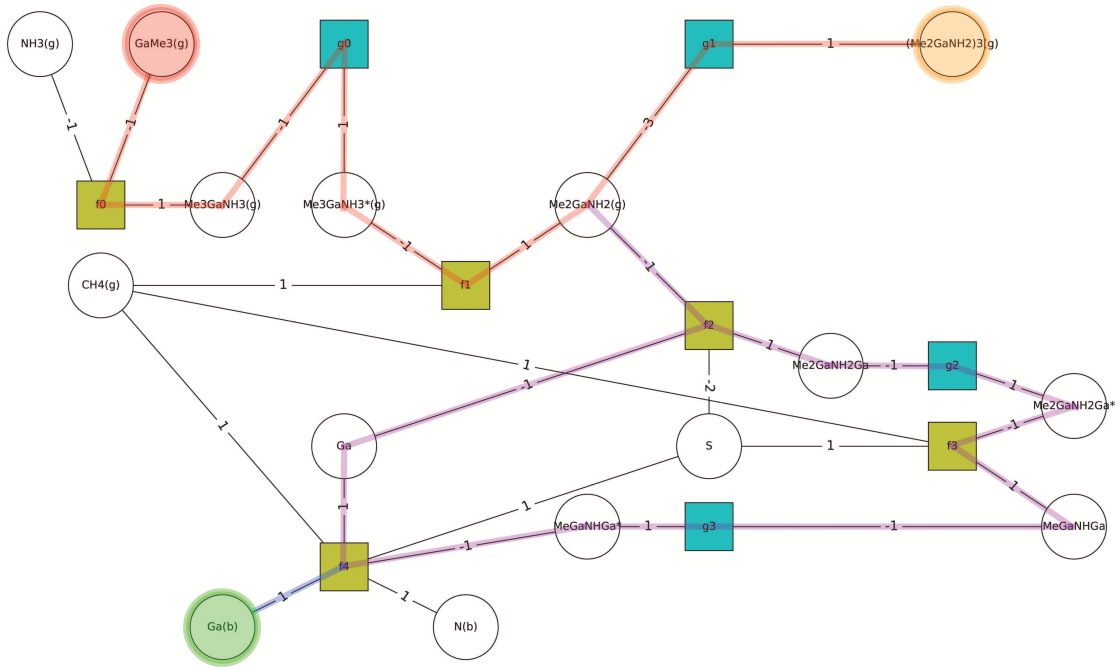

Figure 5.10: S-R graph for the conservation of gallium in GaN CVD

for the two Gallium atoms present on all the surface gallium species, we have the purple line complete a circular loop before undergoing a reaction branch at f_4 to form the bulk phase gallium. The invariant formulated from the S-R graph can be written as,

$$GaMe_3(g) + Me_3GaNH_3(g) + Me_3GaNH_3^*(g) + Me_2GaNH_2{}^{(1)}(g)$$

$$+ (Me_2GaNH_2)_3(g) \quad (Red \quad line)$$

$$+ Me_2GaNH_2{}^{(2)}(g) + Me_2GaNH_2Ga + Me_2GaNH_2Ga^* + MeGaNHGa$$

$$+ MeGaNHGa^* \quad (purple \quad line)$$

$$+ Me_2GaNH_2Ga + Me_2GaNH_2Ga^*$$

$$+ MeGaNHGa + MeGaNHGa^* + Ga \quad (purple \quad line \quad with \quad closed \quad loop)$$

$$+ Ga(b) = constant \quad (blue \quad line)$$

5.2.2 Nitrogen conservation

To understand nitrogen conservation from the S-R Graph we have precursor NH_3(g) (a species node) which forms the adduct and traverses through the system via the surface species and finally ends up with the nitrogen in the bulk phase. The extracted invariant can be written in the string form as,

$$GaMe_3(g) + Me_3GaNH_3(g) + Me_3GaNH_3^*(g) + Me_2GaNH_2{}^{(1)}(g)$$

$$+ (Me_2GaNH_2)_3(g) \quad (Red \quad line)$$

$$+ Me_2GaNH_2{}^{(2)}(g) + Me_2GaNH_2Ga + Me_2GaNH_2Ga^* + MeGaNHGa$$

$$+ MeGaNHGa^* + N(b) = Constant \quad (purple \quad line)$$

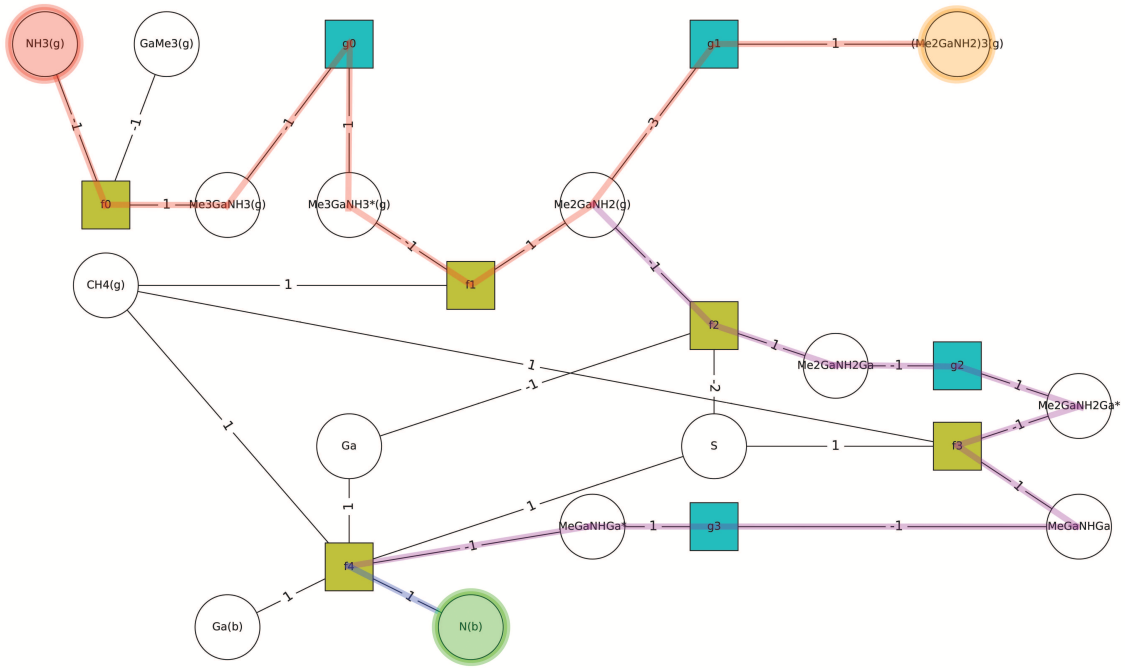

Figure 5.11: S-R graph for the conservation of nitrogen in GaN CVD

5.2.3 Methyl conservation

We have the TMGa forming the adduct and then the red path ends at CH_4 which is generally written as the partial molar amount $CH_4^{(1)}$. The purple line and the blue line result in the other partial molar fractions so that $CH_4 = CH_4^{(1)} + CH_4^{(2)} + CH_4^{(3)}$. In addition we also have the green line accounting for the trimer formation through the species branching.

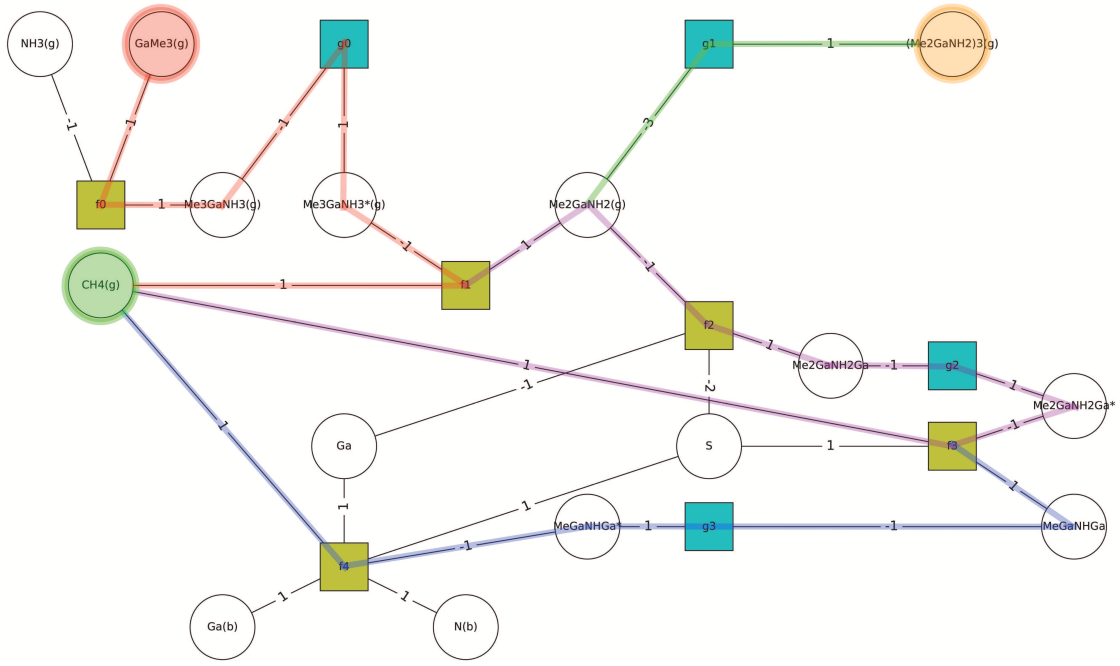

Figure 5.12: S-R graph for the conservation of methyl in GaN CVD

$$GaMe_3(g) + Me_3GaNH_3(g) + Me_3GaNH_3^*(g) + CH_4^{(1)}(g) \quad (Red \quad line)$$

$$+ Me_2GaNH_2{}^{(1)}(g) + (Me_2GaNH_2)_3(g) \quad (Green \quad line)$$

$$+ Me_2GaNH_2{}^{(2)}(g) + Me_2GaNH_2Ga + Me_2GaNH_2Ga^* + CH_4^{(2)}(g) \quad (Purple \quad line)$$

$$+ MeGaNHGa + MeGaNHGa^* + CH_4^{(3)}(g) = constant \quad (Blue \quad line)$$

5.2.4 Hydrogen transfer conservation

The conservation of hydrogen "transfer" is very similar to methyl group. The only difference in the entire invariant pathway is that it begins at ammonia and follows the same path as methyl conservation,

$$NH_3(g) + Me_3GaNH_3(g) + Me_3GaNH_3^*(g) + CH_4^{(1)}(g) \quad (Red \quad line)$$

$$+ Me_2GaNH_2{}^{(1)}(g) + (Me_2GaNH_2)_3(g) \quad (Green \quad line)$$

$$+ Me_2GaNH_2{}^{(2)}(g) + Me_2GaNH_2Ga + Me_2GaNH_2Ga^* + CH_4^{(2)}(g) \quad (Purple \quad line)$$

$$+ MeGaNHGa + MeGaNHGa^* + CH_4^{(3)}(g) = constant \quad (Blue \quad line)$$

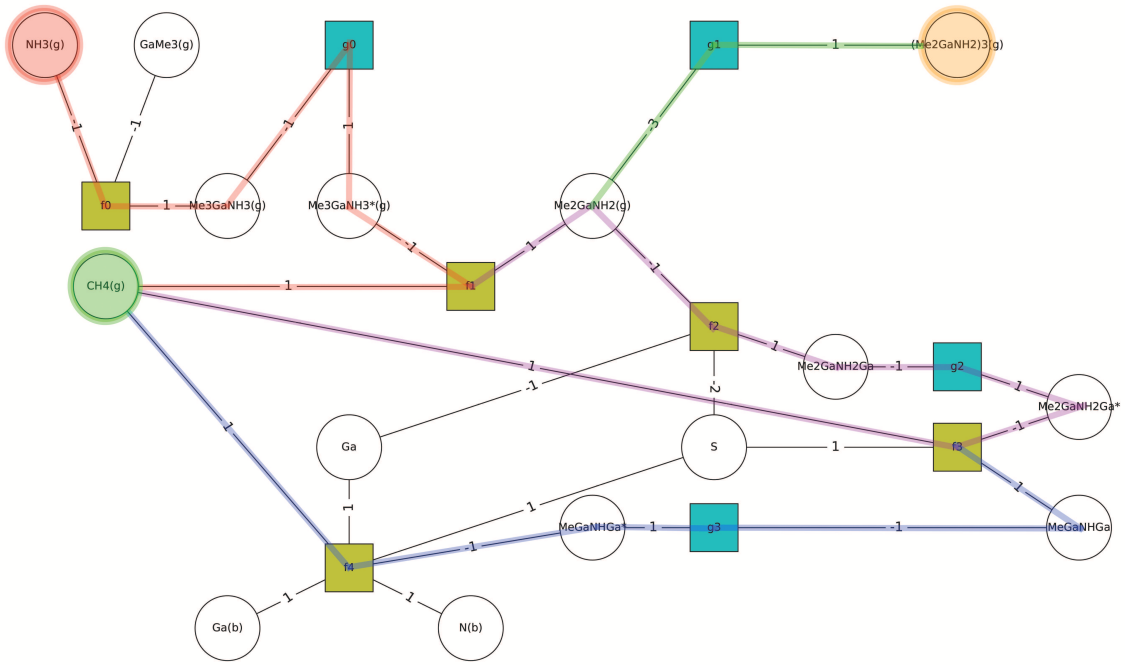

Figure 5.13: S-R graph for the conservation of hydrogen in GaN CVD

5.2.5 Reactive site conservation

So far the conservation of the four physical invariants is very straightforward in terms of looking at species balances. We are left with two more invariants as shown from our Gauss-elimination. The reactive site invariant in the case of CVD has a very similar look to that of an ALD system. We have the sum of all surface

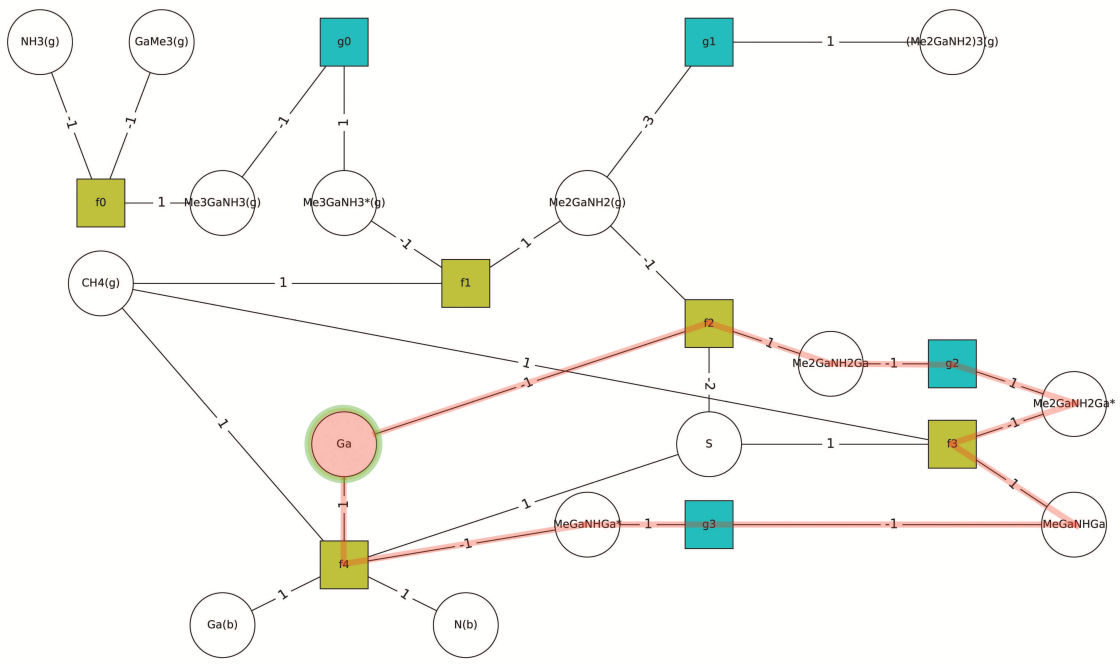

Figure 5.14: S-R graph for the conservation of reactive sites in GaN CVD

species adding up to form a closed loop. However, in a CVD we do not have half cycles unlike ALD. The cycle can be broken into the form of terminal to terminal species beginning at gallium which is the surface site on which the adsorption of the adduct takes place and terminating when its regenerated. We can also see that the reactions f_2 and f_4 which are nothing but the adsorption reaction for the gas phase monomer on the surface and the densification reaction for the surface species to make it into the bulk film respectively are always involved in the reactive site conservation loop. The importance of this invariant is that it makes sure that the reaction surface remains bounded without it growing indefinitely or vanishing. Since we do not have half cycles, we do not have a self limiting behavior in the case of a CVD system. Thus in a steady state CVD as long as there is continuous regeneration of the reactive site 'Ga' we have growth of the crystalline film. The invariant species

string extracted from the S-R graph can be written as,

$$Ga^{(1)} + Me_2GaNH_2Ga + Me_2GaNH_2Ga^* + MeGaNHGa + MeGaNHGa^* + Ga^{(2)} = constant$$

5.2.6 Surface site conservation

We have two cycles starting and ending with S. One of the cycles (in red) consumes two S to form the surface species Me_2GaNH_2Ga which is transformed to a critical complex $Me_2GaNH_2Ga^*$ before releasing a CH_4 with the subsequent regeneration of the Surface site S. The other cycle also represents a similar pathway through the formation of the complex $MeGaNHGa^*$. An overall surface site conservation for a reactor operating at a steady state shows that we always have one or more cycles always containing species S to maintain open adsorption sites for the CVD precursors.

$$S^{(1)} + Me_2GaNH_2Ga + Me_2GaNH_2Ga^* \quad (Red \quad line)$$

$$S^{(2)} + MeGaNHGa + MeGaNHGa^* = constant \quad (Purple \quad line)$$

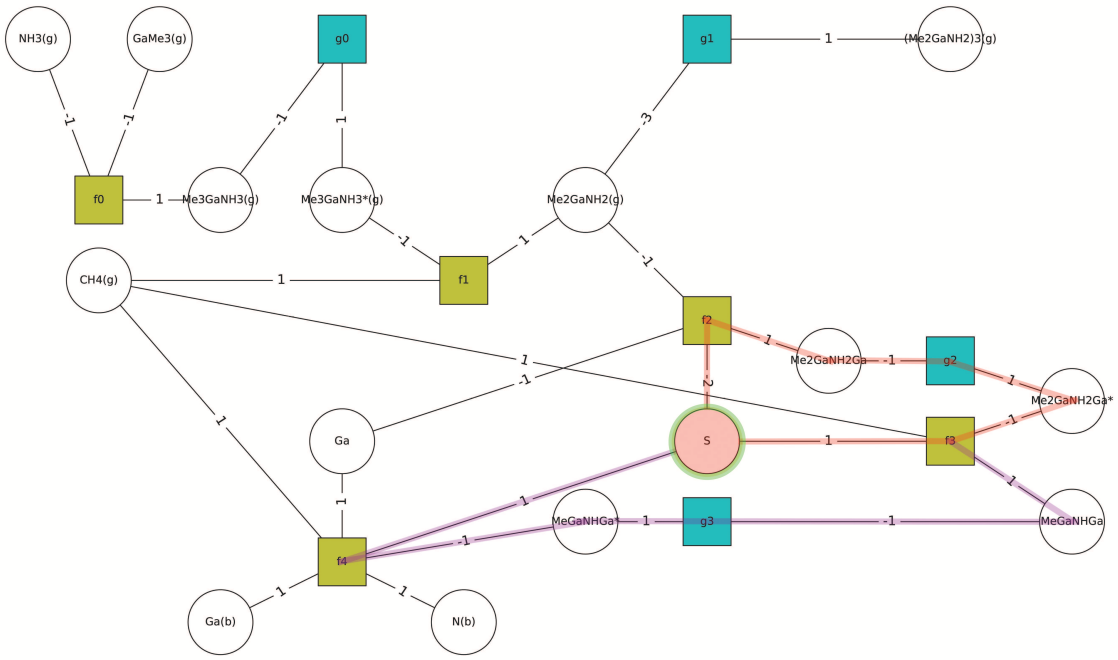

Figure 5.15: S-R graph for the conservation of surface site in GaN CVD

Chapter 6: Conclusions and Future work

The thesis set out to develop a complete set of reaction network analysis tools to analyze thin-film deposition processes through the interpretation of process invariants. Both the reaction factorization as well as the S-R graph approach were performed for ALD and CVD processes. The first part of the thesis helped us successfully separate out the finite and the equilibrium timescales involved in our deposition process. We were also able to identify the redundant dynamic modes as reaction invariants. In both cases factorization technique yielded six independent invariants. However in order to understand the physical meaning of the process invariants we had to focus on applying the rules of the S-R graphs to GaAs and GaN system.

The S-R graph clearly showed that all individual elemental balances (four in each case!) were satisfied at any given point during the course of the reaction. The idea of the "proper" ALD or/and CVD were answered by understanding the two site conservation invariants. In conclusion we need to make a clear distinction between what the two site conservation invariants mean for the ALD and CVD processes. In an ALD process we see that it conformed to self-limiting behavior and growth surface stability while in the CVD of GaN it showed steady state deposition and growth

surface stability. The reactive sites conservation in both processes correspond to growth surface stability. However, the presence of half cycles in ALD differentiates it from a CVD and makes it self-limiting in nature which can be clearly seen in their respective surface site conservation invariants. In addition to these we can also see that the stoichiometry of the deposited film is independent of the reaction rates further asserting our idea to identify a mechanism as "proper" reaction mechanism using the RNA prior to calculating reaction rate values.

Such RNA tools can be used as a preliminary step in understanding deposition mechanisms before performing DFT studies to find out the reaction rates. The scope of this thesis was limited to evaluating reaction invariants and a future work on reaction variant analysis from the perspective of S-R graph should be interesting. It will also be compelling to perform a DFT to evaluate the reaction rates and predict gpc from the variant equations. It is important to note that both our reaction models are considered to be closed systems which does not account for transport of gas phase reactants and byproducts into and from the reactor vessel. An analysis of an open system is necessary before terming our RNA to be complete.

Appendix A: Alternate mechanism for GaAs ALD

Though in the literature it mentions that gallium surface is terminated by methyl groups and the arsenic surface is terminated by hydrogens, it does not clearly explain how many methyl or hydrogen atoms were observed on the surface. Thus, there is a possible second mechanism which is similar to the earlier mechanism except for the differences in the number of hydrogen and methyl groups on the surface.

The first few reactions are very similar to that of the first reaction mechanism, there is adsorption of the TMGa group onto the lone pair on arsenic on the surface followed by a H-transfer reaction resulting in the formation of a Ga-rich surface saturated by the presence of two methyl groups on each gallium.

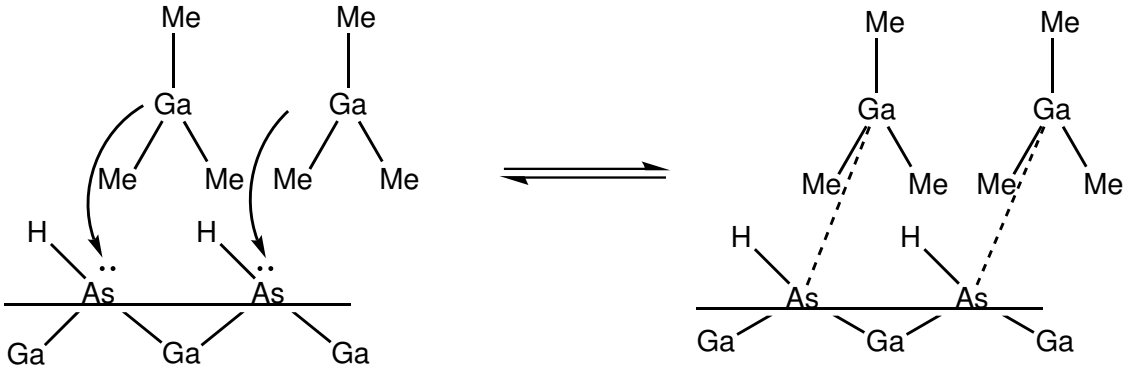

Figure A.1: TMG adsorption on the arsenic surface

Then the hydrogen on the surface arsenic undergoes a proton transfer and is

removed along with the methyl group as methane as shown in Figure A.2 .

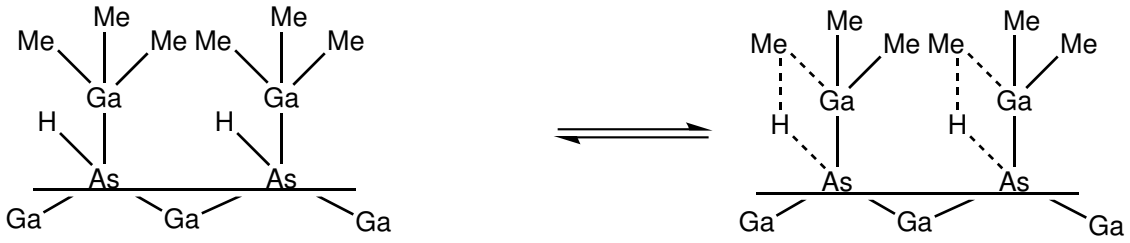

Figure A.2: Transition state before proton removal

Once the methyl group is removed, the gallium has an empty orbital which becomes a surface site for the arsine molecule to adsorb during the second half cycle.

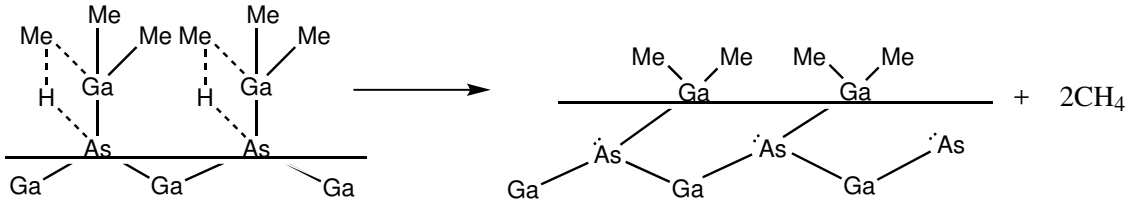

Figure A.3: Proton removal step

It is also important to note that the gallium on the surface now has two methyl groups attached to it as shown in Figure A.3.

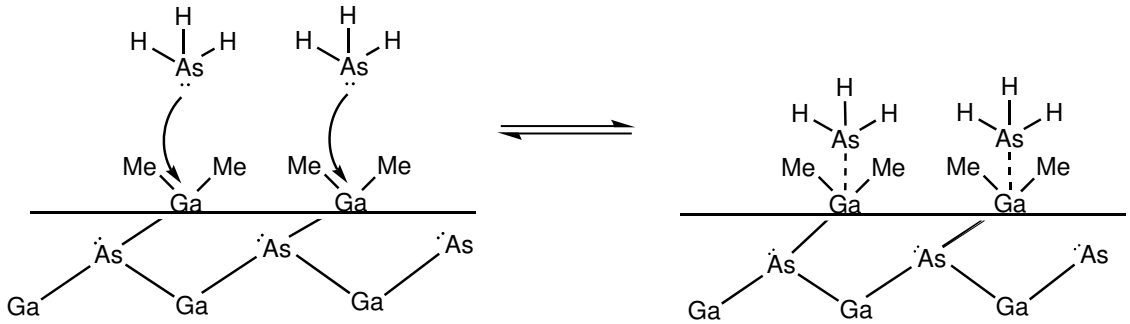

Figure A.4: Arsine adsoprtion on gallium surface site

During the second half cycle the lone pair on the arsine precursor gets adsorbed on the gallium atom as shown in Figure A.4. Another H-transfer reaction results in the elimination of methane to deposit the bulk film and regenerate the orginal arsenic rich reactive site.

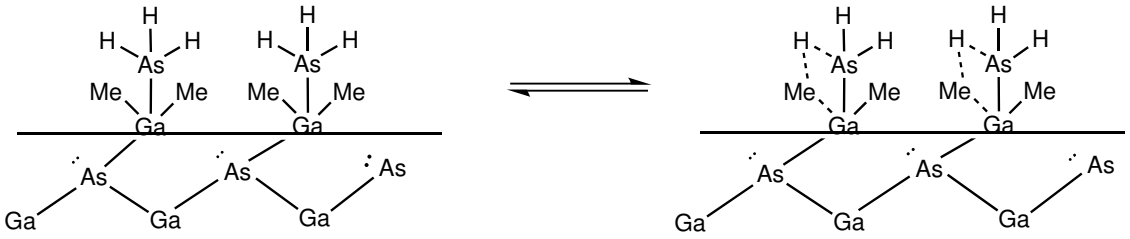

Figure A.5: Transistion state for proton removal

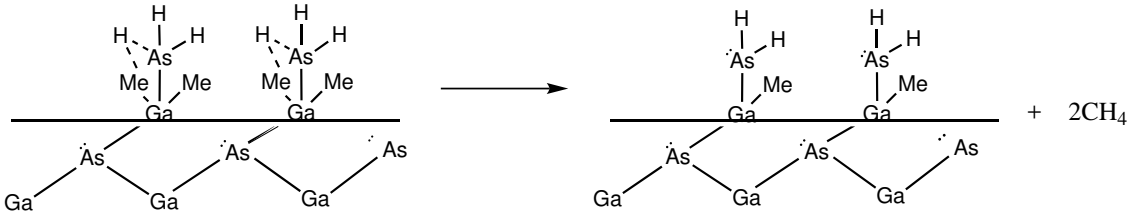

Figure A.6: Formation of an intermediate with a methyl group and two hydrogens

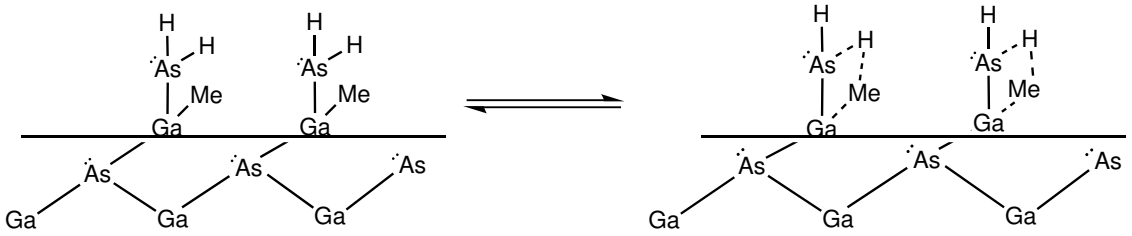

Figure A.7: Transistion state before removal of proton

We now have two reaction mechanism which seem equally plausible. The next challenge then is to identify based on growth per cycle data if we find any one

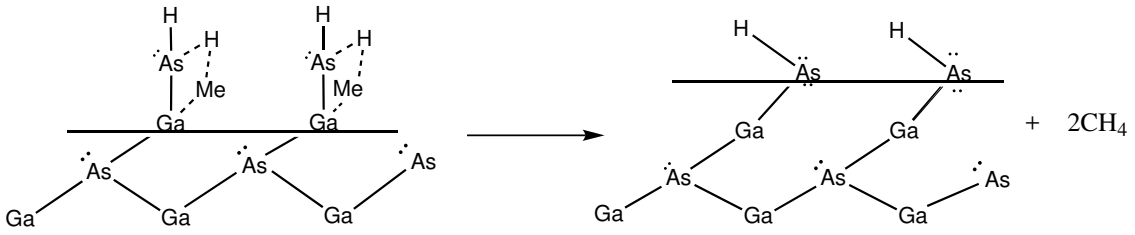

Figure A.8: GaAs in the bulk with regeneration of As surface site

Table A.1: Reaction summary for alternate mechanism of GaAs ALD

Reaction	Rate ($s^{-1}m^{-2}$)
$AsH + GaMe_3\ (g) + 3S \longrightarrow AsHGaMe_3H$	f_0
$AsHGaMe_3H \rightleftharpoons AsHGaMe_3H^*$	$(1/\epsilon)g_0$
$AsHGaMe_3H^* \longrightarrow As\ (b) + GaMe_2 + CH_4\ (g) + S$	f_1
$GaMe_2 + AsH_3\ (g) \longrightarrow GaMe_2AsH_3$	f_2
$GaMe_2AsH_3 \rightleftharpoons GaMe_2AsH_3{}^*$	$(1/\epsilon)g_1$
$GaMe_2AsH_3{}^* \longrightarrow GaMeAsH_2 + CH_4\ (g) + S$	f_3
$GaMeAsH_2 \rightleftharpoons GaMeAsH_2{}^*$	$(1/\epsilon)g_2$
$GaMeAsH_2{}^* \longrightarrow Ga\ (b) + AsH + CH_4\ (g) + S$	f_4

mechanism to be more convincing than the other. By using surface chemistry studies we try to identify the approximate gpc for each of the mechanisms. We can then compare them to gpc data available from litreature [Kaariainen et al., 2013] [Stringfellow, 1991]. Experiments done in [Kaariainen et al., 2013] shows monolayer growth even at high precursor concentrations, and it is achieved when the temperature is between 400-550 °C, which is the temperature of any typical ALD. If we try to estimate the gpc of both mechanism based on our knowledge of the number

of gallium atoms and methyl groups on the surface, it will give us a clearer picture about the more preferred mechanism. Since we have the same surface site in both mechanisms, the number density of surface sites at the beginning of each half cycle is still the same. We consider the surface sites to be gallium, and we have either one or two methyl groups on the surface based on the mechanism. The number of surface sites is the product of the number density with the monolayer thickness of GaAs which is then given by,

$$\begin{aligned}\rho_N &= \frac{\rho_{GaAs}.N_A}{M_{GaAs}} \times \delta z \\ &= \frac{5.32 \times 10^{-21} \frac{g}{nm^3} \times 6.023 \times 10^{23} \frac{atoms}{mol}}{144.645 \frac{g}{mol}} \times 0.28nm \\ &= 6.26 \, \frac{atoms}{nm^2}\end{aligned}$$

We can also calculate the number of methyl groups adsorbed on the surface assuming that our reaction describes complete monolayer growth per cycle, we need to account for the adsorption of six methyl groups for the mechanism proposed and twelve methyl groups (two methyl groups for each Ga atom!) for the alternate mechanism in order to achieve 1 ML gpc. However, the bulkiness of these methyl groups restricts the space they can occupy. We calculate the maximum possible number of methyl groups that can be fit into a nm^2 of surface. The calculation of the area occupied by any ligand was computed by [Puurunen, 2003] with the expression

$$a_L = 2\sqrt{3}{r_L}^2$$

with the assumption of a spherical ligand, where r_L is the radius of the ligand, which in our case is the methyl group. From literature we can see that this value of

$r_L = 0.2nm$. If we divide this quantity by $1nm^2$ we get 7.22 which is the number of methyl groups that can get adsorbed on the surface site.

$$\begin{aligned} a_{CH_3} &= 2\sqrt{3} \times (0.2)^2 \\ &= 0.1386 \, \frac{nm^2}{methyl} \end{aligned}$$

$$\begin{aligned} Number\, of\, Methyl\, groups\, per\, nm^2 &= \frac{1\, nm^2}{0.1386 \, \frac{nm^2}{methyl}} \\ &= 7.22\, methyl\, groups \end{aligned}$$

Since we need six methyl groups to achieve one ML gpc in our proposed mechanism for GaAs and we can accommodate a maximum of 7.22 methyl groups, it seems a much more reasonable mechanism compared to the alternate one which requires 12 methyl groups to achieve 1 ML gpc. However for temperatures and pressures which do not correspond to 1 ML gpc there is high possibility of both these mechanism competing resulting in a much more complicated one.

Bibliography

[Adomaitis, 2016a] Adomaitis, R. A. (2016a). Dynamic dimension reduction for thin-film deposition reaction network models. In *11th IFAC Symposium on Dynamics and Control of Process Systems, including Biosystems (DYCOPS-CAB 2016)*. IFAC.

[Adomaitis, 2016b] Adomaitis, R. A. (2016b). Dynamic order reduction of thin-film deposition kinetics models: A reaction factorization approach. *J. Vac. Sci. Technol. A*, 34:01A104.

[Adomaitis, 2017] Adomaitis, R. A. (2017). Reaction path analysis for atomic layer deposition processes. In *Foundations of Computer Aided Process Operations / Chemical Process Control*. (FOCAPO / CPC 2017).

[Almond et al., 1992] Almond, M., Jenkins, C., and D.A. Rice, K. H. (1992). Organometallic precursors to the formation of gan by mocvd: structural characterisation of me3ga-nh3 by gas-phase electron diffraction. *J. Organomet. Chem.*, 439:251.

[Ars et al., 1998] Ars, R., Watkins, S. P., Yeo, P., Horley, G. A., OBrien, P., and Jones, A. C. (1998). Growth mechanisms in atomic layer epitaxy of gaas. *J. Appl. Phys.*, 83:3390.

[Bandic et al., 1998] Bandic, Z., Piquette, E., Bridger, P., Beach, R., Kuech, T., and Mcgill, T. (1998). Nitride based high power devices: design and fabrication issues. *Solid State Electron*, 42:2289.

[Burk et al., 1999] Burk, A. J., OLoughlin, M., Siergiej, R., Agarwal, A., Sriram, S., Clarke, R., MacMillan, M., Balakrishna, V., and Brandt, C. (1999). Sic and gan wide bandgap semiconductor materials and devices. *Solid State Electron*, 43:1459.

[Craciun and Feinberg, 2006] Craciun, G. and Feinberg, M. (2006). Multiple equilibria in complex chemical reaction networks: Ii. the species-reaction graph. *SIAM J. Appl. Math.*, 66:1321–1338.

[Creighton and Bansenauer, 1993] Creighton, J. R. and Bansenauer, B. A. (1993). The surface chemistry and kinetics of gaas atomic layer epitaxy. *Thin Solid Films*, 225:17–25.

[Daoutidis, 2015] Daoutidis (2015). Surveys in differential-algebric equations. In Ilchmann, A. and Reis, T., editors, *DAE's in model reduction of chemical process: An Overview*. Springer International Publishing.

[Johnson et al., 2014] Johnson, R. W., Hultqvist, A., and Bent, S. F. (2014). A brief review of atomic layer deposition: from fundamentals to applications. *Materials Today*, 17:236–246.

[Kaariainen et al., 2013] Kaariainen, T., Cameron, D., Kaariainen, M.-L., and Sherman, A. (2013). *Atomic Layer Deposition of Nanostructured Materials*. Wiley, 2 edition.

[Maa and Dapkus, 1993] Maa, B. Y. and Dapkus, P. D. (1993). Study of surface reactions in atomic layer epitaxy of gaas using trimethylgallium by reflectance difference spectroscopy and mass spectroscopy. *Thin Solid Films*, 225:12–16.

[Mazzarese et al., 1989] Mazzarese, D., Tripathi, A., Conner, W., Jones, K., Calderon, L., and Eckart, W. (1989). In situ ftir and surface analysis of the reaction of trimethylgallium and ammonia. *J. Electron. Mater.*, 18:369.

[Mihopoulos, 1999] Mihopoulos, T. (1999). *Reaction pathways in organometallic chemical vapor deposition of AlGaN*. PhD thesis, Massachusetts Institute of Technology, Chemical Engineering Department.

[Nishiwaza et al., 1987] Nishiwaza, J., Kurabayashi, T., Abe, H., and Nozoe, A. (1987). Mechanisms of surface reaction in gaas layer growth. *Surface Sciences*, 185:249–268.

[Parikh and Adomaitis, 2006] Parikh, R. and Adomaitis, R. (2006). An overview of gallium nitride growth chemistry and its effect on reactor design: Application to a planetary radial-flow cvd system. *Journal of Crystal Growth*, 286:259–278.

[Pawlowski et al., 2000] Pawlowski, R., Theodoropoulos, C., Salinger, A., Mountziaris, T., Moffat, H., Shadid, J., and Thrush, E. (2000). Fundamental models of the metalorganic vapor-phase epitaxy of gallium nitride and their use in reactor design. *J. Crystal Growth*, 221:622.

[Pinna and Knez, 2011] Pinna, N. and Knez, M. (2011). *Atomic Layer Deposition of Nanostructured Materials*. Wiley.

[Puurunen, 2003] Puurunen, R. L. (2003). Growth per cycle in atomic layer deposition: A theoretical model. *Chem. Vap. Deposition*, 5:9.

[Remmers et al., 2015] Remmers, E. M., Travis, C. D., and Adomaitis, R. A. (2015). Reaction factorization for the dynamic analysis of atomic layer deposition kinetics. *Chemical Engineering Science*, 127:374–391.

[Safvi et al., 1997] Safvi, S., Redwing, J., Tischler, M., and Kuech, T. (1997). Gan growth by metallorganic vapor phase epitaxy. *J. Electrochem. Soc.*, 144:1789.

[Stringfellow, 1991] Stringfellow, G. B., editor (1991). *Gallium Arsenide and related compounds, Proceedings of the eighteenth International Symposium on Gallium Arsenide and related compounds*, 120. Institute of physics, IOP publishing Ltd.

[Sun et al., 1999] Sun, J., Redwing, J., and Kuech, T. (1999). Transport and reaction behaviors of precursors during metalorganic vapor phase epitaxy of gallium nitride. *Phys. Stat. Sol. (a)*, 176:693.

[Sun et al., 2000] Sun, J., Redwing, J., and Kuech, T. (2000). Model development of gan movpe growth chemistry for reactor design. *J. Electron. Mater.*, 29:2.

[Theodoropoulos et al., 2001] Theodoropoulos, C., Mountziaris, T., Moffat, H., and Han, J. (2001). Design of gas inlets for the growth of gallium nitride by metalorganic vapor phase epitaxy. *J. Crystal Growth*, 217:65.

[Tischler and Bedair, 1986] Tischler, M. A. and Bedair, S. M. (1986). Selflimiting mechanism in the atomic layer epitaxy of gaas. *Appl. Phys. Lett.*, 48:1681.

[Wei and Prater, 1962] Wei, J. and Prater, C. (1962). The structure and analysis of complex reaction systems. *Adv. Catalysis*, 13:203–392.

[Yu, 1993] Yu, M. L. (1993). Mechanisms of atomic layer epitaxy of gaas. *J. Appl. Phys.*, 73:716.

Conferences and Publications

Hossein Salami, Krishnaprasath Ramakrishnan and Raymond A. Adomaitis , "*Reaction Network Analysis for Thin-Film Deposition Processes: Physical Interpretation of Reaction Invariants*", conference paper presented at the American Institute of Chemical Engineers (AIChE) 2016.

Hossein Salami, Krishnaprasath Ramakrishnan, Raymond A. Adomaitis, "Reaction Path Analysis for ALD and CVD processes", *Adv.Materials Interfaces* (2017) (under preparation).